arXiv:2204.13657v2 [quant-ph] 30 May 2022

Dynamical purification and the emergence of quantum state designs from the projected ensemble

Matteo Ippoliti and Wen Wei Ho
Department of Physics, Stanford University, Stanford, CA 94305, USA
(Dated: June 1, 2022)

Quantum thermalization in a many-body system is defined by the approach of local subsystems towards a universal form, describable as an ensemble of quantum states wherein observables acquire thermal expectation values. Recently, it was demonstrated that the *distribution* of these quantum states can also exhibit universal statistics, upon associating each state with the outcome of a local projective measurement of the complementary subsystem. Specifically, this collection of pure quantum states – called the projected ensemble – can under certain conditions mimic the behavior of a maximally entropic, uniformly random ensemble, i.e. form a *quantum state-design*, representing a "deeper" form of quantum thermalization. In this work, we investigate the dynamical process underlying this novel emergent universality. Leveraging a space-time duality mapping for one-dimensional quantum circuits, we argue that the physics of dynamical purification, which arises in the context of monitored quantum systems, constrains the the projected ensemble's approach towards the uniform distribution. We prove that absence of dynamical purification in the space-time dual dynamics (a condition realized in dual-unitary quantum circuits with appropriate initial states and final measurement bases) generically yields exact state-designs for all moments k at the same time, extending previous rigorous results [Ho and Choi, Phys. Rev. Lett. **128**, 060601 (2022)]. Conversely, we show that, departing from these conditions, dynamical purification can lead to a separation of timescales between the formation of a quantum state-design for moment $k = 1$ (regular thermalization) and for high moments $k \gg 1$ ("deep" thermalization). Our results suggest that the projected ensemble can probe nuanced features of quantum dynamics inaccessible to regular thermalization, such as quantum information scrambling.

I. INTRODUCTION

Generic isolated quantum many-body systems are expected to thermalize under their own dynamics. That is, such systems are believed to relax locally to a steady state given by a maximally entropic mixed state, up to constraints from global conservation laws [1–3]. This universal behavior arises because of the build-up of entanglement between a local subsystem and its complement, which serves as a 'bath': upon ignoring the state of the latter, the former is captured by a reduced density matrix describing a statistical mixture of different configurations that has a universal form (the Gibbs ensemble).

Recently, a new perspective on describing a local subsystem of a quantum many-body system was put forth by Ref. [4, 5]. Instead of ignoring the state of the bath, it is assumed that some knowledge of the bath's effect on the subsystem can be retained by the observer. Concretely, one can study a collection of *pure states* of a local subsystem A, each of which is associated with the restriction of the global wavefunction to A, following a Born update due to a projective measurement of the complementary subsystem in a fixed, local basis. These projected states together with their respective probabilities form the so-called *projected ensemble*, and can be thought of as 'unraveling' the reduced density matrix in terms of its constituent pure states according to an observation of the bath. Notably, this goes beyond the standard framework of quantum thermalization, which depends solely on the reduced density matrix itself.

Intriguingly, Refs. [4, 5] found evidence of a novel universal behavior exhibited by the projected ensemble. In particular, it was observed through numerics and experiments that under quench dynamics of generic quantum-chaotic many-body systems without conservation laws or at infinite temperature, the distribution of projected states approaches that of a uniformly (i.e., unitarily-invariant, or Haar) random ensemble, independent of microscopic details, with an accuracy that increases with the bath size and the quench time. In quantum information theoretic language, the projected ensemble is said to approach a *quantum state-design* [6, 7]. This behavior implies that the statistics of the local subsystem tends towards a maximally entropic distribution not just at the level of expectation values of local observables, but rather at the level of the Hilbert space. Thus, it can be viewed as a stronger notion of quantum thermalization.

Subsequent work has established this novel phenomenon more firmly. An exactly-solvable instance of this behavior was provided in Ref. [8], which analyzed the non-integrable kicked Ising model (KIM) in certain parameter regimes and rigorously proved the emergence of *exact* quantum state-designs at finite time in quench dynamics. The proof leveraged the so-called *dual-unitarity* of the KIM—the property that its representation as a quantum circuit in $(1+1)$-dimensional space-time is unitary along both the time and space directions. The projected states can thus be understood as arising from different unitary evolutions in the space direction, indexed by measurement outcomes on the bath; it was further shown that the unitary operators corresponding to the different measurement outcomes densely fill the unitary group (in the infinite-bath limit), giving rise to a quan-

tum state-design. Ref. [9] further provided constructions of a class of quantum circuits that can be analyzed in similar fashion as the KIM, strongly suggesting the emergence of exact quantum state designs in these models too.

Despite such progress, much remains to be understood of this newly uncovered nonequilibrium universality. An interesting question is to characterize in finer detail the dynamical process of "deep" thermalization, defined by the formation of higher state designs in the projected ensemble . To this end one can consider the time t_k at which the projected ensemble's distribution approaches the uniformly-random one at the level of its k-th moment (within some small fixed accuracy, measured using an appropriate norm, see Sec. II A 3)—that is, the time taken to form an (approximate) *quantum state k-design* [6, 7]. For this reason we refer to $\{t_k\}$ as the "design times". Note that as the first moment ($k = 1$) of the projected ensemble is precisely the reduced density matrix, t_1 is the time taken for regular thermalization to occur. The design times are by definition non-decreasing in k, and for the models numerically probed in Ref. [5], were generically found to increase with k. On the other hand, Ref. [8] found that for the KIM in the thermodynamic limit, remarkably, all design times were finite and furthermore coincided, being exactly equal to the subsystem size N_A. In other words, in this model, when regular thermalization (convergence of the $k = 1$ moment) occurs, "deep" thermalization (convergence of the $k > 1$ moments) occurs concurrently. This immediately raises questions about the origin of these different behaviors, and more generally, what physics sets the separation in timescales between regular thermalization and "deep" thermalization.

In this article, we make progress on these questions in two ways, focusing on dynamics in one spatial dimension. First, we prove that the dynamics of quantum circuits comprised of random local dual-unitary gates, with a suitable choice of compatible initial states and local measurement basis on the bath, *almost always* reproduce the KIM behavior, namely they form exact state k-designs for all k at the thermalizaton time $t_1 = N_A$. This extends the scope of the conclusions in Refs. [8, 9] and reveals that *universality* of the gate set (i.e. its ability to approximate arbitrary unitaries [10]) plays a key role alongside dual-unitarity. Second, we show that if the above assumptions (of dual-unitarity and compatible initial states/measurement basis) are violated, then higher design times $t_{k>1}$ can be separated from the regular thermalization time t_1. This separation is a consequence of *dynamical purification* [11], a phenomenon that arises in quantum systems subject to monitoring by an outside observer, whereby an input mixed state gets gradually purified over the course of the dynamics. Such monitored systems have been the focus of much attention lately due to the emergence of entanglement phases and phase transitions in their quantum trajectories [11–15]. In our present case, similar physics applies because the states making up the projected ensemble can be thought of coming from quantum circuit evolutions in the spatial direction (indexed by measurement outcomes) that are now generically non-unitary, unlike in the KIM studied in Ref. [8]. Due to dynamical purification, many of these different trajectories essentially map to the same vector in Hilbert space, leading to a restriction on the ability of the ensemble to uniformly cover the space; with increasing time, this restriction is alleviated.

This result is interesting as it reveals nuances in the different notions of local thermal equilibration in quantum many-body systems. Regular thermalization, captured by the reduced density matrix, only probes the total build-up of entanglement between the subsystem and the bath, and is insensitive to how that entanglement is organized in space. In contrast, "deep" thermalization, captured by higher moments of the projected ensemble, is sensitive to the choice of local measurement basis, and thus to the structure of entanglement in space. This suggests a connection with quantum information scrambling [16–21], the phenomenon by which local operators grow in size over time, spreading quantum information across the system. Importantly, these phenomena can happen on different timescales. For example, chaotic systems feature an "entanglement velocity" v_E governing the ballistic growth of entanglement (and thus thermalization) [22, 23] and a "butterfly velocity" v_B governing scrambling [19, 20, 24]. In this work we identify yet another quantity, the "purification velocity" v_p, bounding the formation of high designs.

Before proceeding, let us remark that Ref. [25] already establishes a sharp connection between the onset of regular thermalization and the simultaneous formation of higher designs: whenever the reduced density matrix on A is close to being maximally mixed (i.e., at infinite temperature), then with high probability the projected ensemble forms an approximate quantum state-design, provided the measurement basis of the complementary subsystem is chosen at random from the Haar measure (which is typically non-local and highly entangled). However, a setting which is arguably more natural for experiments is that of *spatially local* measurement bases, like the ones we consider in this work. Such bases are highly atypical (with respect to the Haar measure), and thus they can evade the result of Ref. [25], enabling nontrivial separations between the different design times.

The rest of the paper is organized as follows. In Section II we review the projected ensemble formalism, as well as the concepts of space-time duality and dynamical purification in monitored systems which are important technical tools in this work. Section III contains our first main result, a proof of the emergence of exact state designs in random dual-unitary circuits. In Section IV we move away from dual-unitarity and present our second main result, an analytical connection between design formation and dynamical purification. Finally, we discuss our results and outline directions for future work in Sec. V.

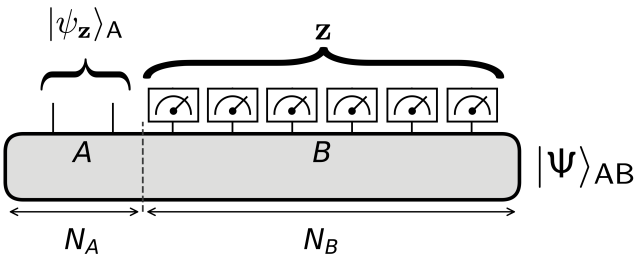

FIG. 1. The projected ensemble: a global state $|\Psi\rangle$ on a composite system AB is projectively measured in B, yielding a pure state $|\psi_{\mathbf{z}}\rangle$ on A (Eq. 6) with probability $p(\mathbf{z})$ (Eq. 5), indexed by the measuremet outcome $\mathbf{z}$. The collection $\{p(\mathbf{z}), |\psi_{\mathbf{z}}\rangle\}$ constitutes the projected ensemble on A.

II. OVERVIEW OF RELEVANT CONCEPTS

We first motivate and review the theoretical framework behind the projected ensemble, first introduced by Refs. [4, 5]. We also present a high-level introduction to the concepts of space-time duality (the idea of studying quantum circuits as evolution in the space, rather than time, direction), and monitored quantum dynamics (the dynamics quantum systems evolving under the combined action of unitary transformations and measurements), which will play central roles in our subsequent analysis of the process of "deep" thermalization.

A. The projected ensemble

1. Motivation and definition

Consider a quantum many-body system of spin-1/2 degrees of freedom (qubits)[1] on N sites, described by a pure global wavefunction $|\Psi\rangle$. Suppose we are interested in describing the properties of a local subsystem A, comprised of spins $i = 1, \cdots, N_A$. The conventional approach is to construct the reduced density matrix ρ_A by tracing out the complementary subsystem B (intuitively, the 'bath'):

$$\rho_A = \mathrm{Tr}_B \left(|\Psi\rangle\langle\Psi| \right), \tag{1}$$

in which expectation values of observables O supported on region A can be computed via

$$\langle O \rangle = \mathrm{Tr} \left(\rho_A O \right). \tag{2}$$

If $|\Psi\rangle = |\Psi(t)\rangle$ is a state obtained in dynamics, then studying how expectation values of local observables settle to an equilibrium value, $\langle O(t) \rangle \to \langle O \rangle_{\mathrm{eq.}}$, is equivalent to studying how the reduced density matrix relaxes to an equilibrium ensemble, $\rho_A(t) \to \rho_{\mathrm{eq.}}$. According to the general statistical-mechanical principle of maximization of entropy, we expect $\rho_{\mathrm{eq.}}$ to be given by a Gibbs state parameterized by Lagrange multipliers corresponding to different globally conserved quantities (modulo ergodicity-breaking scenarios like many-body localization [26, 27]). In particular, with only energy conservation, this takes the form

$$\rho_{\mathrm{eq.}} \propto \mathrm{Tr}_B \left(e^{-\beta H} \right), \tag{3}$$

where β is the inverse temperature set by the conserved energy of the initial state. We refer to such an equilibriation scenario as "regular thermalization".

The formalism of a reduced density matrix as a description of local properties of a subsystem is complete, but importantly under the assumption that knowledge of the complementary subsystem B is inaccessible (or lost) to the observer. However, in a new generation of experimental systems—quantum simulators [28]—this assumption need not always hold. For example, in systems like cold atoms in optical lattices with quantum gas microscopes, individually trapped Rydberg atoms or ions, and superconducting circuits, microscopic read-out of the entire system is routinely performed, whereupon global *bit-strings* $\mathbf{Z} \in \{0,1\}^N$ are collected. By splitting such a bit-string into its restrictions to subsystems A and B, $\mathbf{Z} = (\mathbf{z}_A, \mathbf{z}_B)$ with $\mathbf{z}_A \in \{0,1\}^{N_A}$ and $\mathbf{z}_B \in \{0,1\}^{N_B}$ (here $N = N_A + N_B$), we gain a joint classical snapshot of the states of both the subsystem of interest and the bath; in other words, *correlations* between the subsystem and bath are directly accessible. Explicitly, statistics of the subsystem A can be studied *conditioned* upon observing state $\mathbf{z}_B$ of the bath B. Such information cannot be captured solely by the reduced density matrix and necessitates the development of a new theoretical framework.

The *projected ensemble* formalism precisely achieves this goal. We consider the case of projective measurements performed in the computational basis—which, as we argued above, is of practical relevance to quantum simulators—but we note this assumption can be relaxed to allow for other choices too (as we will do later, and as was also considered in [9, 25]). Concretely, a measurement outcome on B will be labeled by a bit-string $\mathbf{z} \in \{0,1\}^{N_B}$ (we drop the subscript in $\mathbf{z}_B$ for convenience), so that following the measurement, the global wavefunction is updated according to the Born rule as

$$|\Psi\rangle \mapsto \left(\mathbb{I}_A \otimes |\mathbf{z}\rangle\langle\mathbf{z}|_B \right) |\Psi\rangle / \sqrt{p(\mathbf{z})}, \tag{4}$$

which occurs with probability

$$p(\mathbf{z}) = \langle\Psi| \left(\mathbb{I}_A \otimes |\mathbf{z}\rangle\langle\mathbf{z}|_B \right) |\Psi\rangle. \tag{5}$$

Consequently, the state on A will be in a *pure* state indexed by the measurement outcome $\mathbf{z}$,

$$|\psi_{\mathbf{z}}\rangle = \left(\mathbb{I}_A \otimes \langle\mathbf{z}|_B \right) |\Psi\rangle / \sqrt{p(\mathbf{z})}. \tag{6}$$

[1] Though we have specialized to qubit systems here, note that all discussions and results extend straightforwardly to the more general case of qudits or fermions.

The projected ensemble is then defined to be the set of such pure states and their respective probabilities indexed by $\mathbf{z} \in \{0,1\}^{N_B}$:

$$\mathcal{E} := \{p(\mathbf{z}), |\psi_{\mathbf{z}}\rangle\}, \tag{7}$$

which is a probability distribution on the Hilbert space $\mathcal{H}_A$ of A.

2. *Moments of the projected ensemble and their information content*

A probability distribution may be characterized by its moments. For the projected ensemble, the k-th moment is captured by the object

$$\rho^{(k)} = \sum_{\mathbf{z}} p(\mathbf{z}) \left(|\psi_{\mathbf{z}}\rangle\langle\psi_{\mathbf{z}}|\right)^{\otimes k}, \tag{8}$$

which is a density matrix defined on k replicas of the Hilbert space $\mathcal{H}_A$. It can be readily verified that the mean, $k = 1$, is the reduced density matrix $\rho^{(1)} = \rho_A$. An example of information captured by the projected ensemble but not by the reduced density matrix is the quantity

$$\mathbb{E}_{\mathcal{E}}\left[\langle O\rangle_{\mathbf{z}}^2\right] \equiv \sum_{\mathbf{z}} p(\mathbf{z}) \left(\langle\psi_{\mathbf{z}}|O|\psi_{\mathbf{z}}\rangle\right)^2, \tag{9}$$

which is related to the ensemble variance of *conditional* expectation values $\langle O\rangle_{\mathbf{z}} = \langle\psi_{\mathbf{z}}|O|\psi_{\mathbf{z}}\rangle$—the expectation of an operator O on A conditioned upon observing the bath in (classical) state $|\mathbf{z}\rangle_B$. This quantity can in fact be expressed as the expected value of a "higher-order" observable evaluated in a specific density matrix on a k-fold replicated space, namely $\mathbb{E}_{\mathcal{E}}\left[\langle O\rangle_{\mathbf{z}}^k\right] = \mathrm{Tr}\left(\rho^{(k)} O^{\otimes k}\right)$, with $k = 2$ (compare this expression to Eq. (2) for a "regular" observable). The quantity in Eq. (9) and its generalizations to higher k have been measured in a Rydberg-atom-based quantum simulator [4], specifically with the choice $O = |\mathbf{s}\rangle\langle\mathbf{s}|_A$, a projector onto bit-string $\mathbf{s} \in \{0,1\}^{N_A}$. This yields information on the probability of observing bit-string $\mathbf{s}$ on A, conditioned upon having observed bit-string $\mathbf{z} \in \{0,1\}^{N_B}$ on the bath.

3. *"Deep" thermalization, quantum state-designs, and design times*

Given that it is believed that the first moment of the projected ensemble $\rho^{(1)} = \rho_A$ tends to a universal equilibrium state $\rho_{\text{eq.}} \propto \mathrm{Tr}_B\left(e^{-\beta H}\right)$ in generic quantum many-body dynamics, an immediate question that arises is if higher moments $\rho^{(k)}$ similarly equilibrate to universal ensembles. In general, the form of such ensembles is not fully known (see however Ref. [29, 30]), but there is a particularly clean limiting scenario that can be considered: the case of systems without symmetries or conservation laws, in which case the principle of maximization of entropy suggests the unitarily-invariant (Haar) ensemble, whose kth moment is given by

$$\rho_H^{(k)} = \int_{\psi\sim\mathrm{Haar}(\mathcal{H}_A)} d\psi \left(|\psi\rangle\langle\psi|\right)^{\otimes k} = \frac{\Pi_{\text{symm}}}{\binom{2^{N_A}+k-1}{k}}, \tag{10}$$

where Π_{symm} is a projector on the symmetric sector of the replicated Hilbert space $\mathcal{H}_A^{\otimes k}$. It is natural to conjecture that in dynamics without explicit conservation laws (like time-periodic systems or quantum circuit dynamics), or in systems at infinite temperature, $\rho^{(k)}$ equilibrates to such a maximally-entropic ensemble, i.e.,

$$\rho^{(k)}(t) \xrightarrow{t\to\infty} \rho_H^{(k)}. \tag{11}$$

For $k = 1$, this reproduces Eq. (3) with $\beta = 0$.

Mathematically, convergence to the uniform ensemble can be quantified by the normalized distance

$$\Delta_\alpha^{(k)} \equiv \frac{\|\rho^{(k)} - \rho_H^{(k)}\|_\alpha}{\|\rho_H^{(k)}\|_\alpha}, \tag{12}$$

where $\|\cdot\|_\alpha$ is the Schatten norm of index α. In quantum information theoretic language, when $\Delta_\alpha^{(k)} = 0$ the ensemble $\mathcal{E}$ of pure states is said to form a *quantum state k-design*, as it is reproducing the kth moment of the Haar random ensemble, Eq. (10) [6, 7]. A property that may be desired of these distances is that they obey *monotonicity*, i.e., that $\Delta_\alpha^{(k+1)} \geq \Delta_\alpha^{(k)}$ for any k. This is desirable because it implies that, if $\mathcal{E}$ is an ϵ-*approximate* quantum state k-design (that is, $\Delta_\alpha^{(k)} \leq \epsilon$), then it is also an ϵ-approximate quantum state k'-design for all $k' \leq k$. In Appendix A we show that the distances defined with the indices $\alpha = 1$ (trace norm), $\alpha = 2$ (Frobenius norm), or $\alpha = \infty$ (operator norm) obey such a property.

The measures defined in Eq. (12) to quantify closeness to a quantum state k-design include one which will be easier to work with analytically, which is based on the so-called *frame potential* of the ensemble $\mathcal{E}$ [6, 18], defined for each k as

$$F^{(k)} \equiv \sum_{\mathbf{z},\tilde{\mathbf{z}}} p_{\mathbf{z}} p_{\tilde{\mathbf{z}}} |\langle\psi_{\mathbf{z}}|\psi_{\tilde{\mathbf{z}}}\rangle|^{2k} = \mathrm{Tr}\left[\left(\rho^{(k)}\right)^2\right]. \tag{13}$$

This is nothing more than the purity of the density matrix $\rho^{(k)}$. Indeed, one can see that for $\alpha = 2$, Eq. (12) yields

$$\left(\Delta_2^{(k)}\right)^2 = \frac{F^{(k)}}{F_H^{(k)}} - 1, \tag{14}$$

where $F_H^{(k)} \equiv \binom{2^{N_A}+k-1}{k}^{-1}$ is the frame potential of the Haar ensemble. It follows that the frame potential obeys the bound

$$F^{(k)} \geq \binom{2^{N_A}+k-1}{k}^{-1} \tag{15}$$

with equality if and only if $\mathcal{E}$ forms an exact quantum state k-design, $\rho^{(k)} = \rho_H^{(k)}$.

Given the above measures of closeness to a uniformly-random ensemble, one may ask about the time taken for the projected ensemble to achieve a given state k-design within some accuracy ϵ over the course of quench dynamics. To this end we can define for each $k \geq 1$, and for each choice of Schatten-index α, a *design time* $t_{k,\alpha}$ as

$$t_{k,\alpha} = \min_t \left(\Delta_\alpha^{(k)}(t) < \epsilon \right), \tag{16}$$

which is the minimum time such that the chosen distance to the uniformly-random ensemble falls below some arbitrarily small threshold $\epsilon > 0$. This definition naturally encompasses the thermalization time, t_1, but also an infinite sequence of higher design times $t_{k>1}$, which may capture features of the dynamics beyond regular thermalization, that we dub "deep" thermalization. Note that from monotonicity of the normalized distances $\Delta_\alpha^{(k)}$ for $\alpha \in \{1, 2, \infty\}$, the design times $t_{k,\alpha}$ for such indices are also monotonic: $t_{k+1,\alpha} \geq t_{k,\alpha}$. Past works on approximate quantum state designs have used $\alpha = 1$ [4, 5] and $\alpha = \infty$ [7, 31]; in this work it will be technically more convenient to use $\alpha = 2$, and we henceforth drop the subscript α with the understanding that we refer to $\alpha = 2$. While we do not expect the choice of α to qualitatively affect the scaling of design times, it would be interesting to investigate this dependence in future work.

In the rest of this paper, we focus on dynamics generated by quantum circuits in one-dimension with gates arranged in a brickwork pattern, which serve as toy-models for quantum many-body dynamics that preserve only the important minimal ingredients of locality and unitary.

B. Space-time duality and dual-unitarity

Recently, significant progress in our understanding of the projected ensemble and the formation of state designs [8, 9] has been achieved through the concept of *space-time duality*. Generally speaking, this is a transformation of one-dimensional quantum circuits that exchanges the roles of space and time in the dynamics [32–39] (recently extended also to higher dimensional circuits [38, 40] as well as continuum field theories [41]). Such an exchange generically breaks unitarity—i.e., the space-time dual of a unitary circuit is typically *not* itself unitary; however, there is a class of models, dubbed *dual-unitary circuits* [42–45], which are unitary in both the space and time directions. This condition provides a great deal of analytical control over the dynamics, and has enabled progress on questions ranging from the emergence of random matrix theory, to the growth of entanglement and the decay of correlation functions in strongly-interacting systems [43–52].

The building blocks of dual-unitary circuits are dual-unitary gates: unitary matrices on two qubits[2], U_{ij}^{kl}, such that their space-time duals $(\tilde{U})_{ij}^{kl} \equiv U_{ik}^{jl}$ are also unitary. This condition defines a submanifold of co-dimension 2 in the unitary group $U(4)$ on two qubits. Neglecting an overall phase, dual-unitary gates on two qubits can be parametrized as [47]

$$\mathfrak{DU} = \{(r_1 s_2)\mathsf{SWAP} e^{-iJZ_1Z_2}(u_1 v_2)\} \tag{17}$$

where $r, s, u, v \in SU(2)$ and $J \in [0, \pi/4]$ (giving a total of 13 parameters), and $\mathsf{SWAP} = e^{i\frac{\pi}{4}\boldsymbol{\sigma}_1\cdot\boldsymbol{\sigma}_2}$ exchanges the state of the two input qubits. In the rest of this work we refer to brickwork circuits of dual-unitary gates as DU.

A notable example of DU circuit is the KIM with couplings tuned to a special point. The analytical results in Ref. [8] on the formation of exact state designs leverage precisely this fact. The key idea is to analyze the quantum circuit that represents the projected ensemble by "segmenting" it into *transfer matrices* that describe a dual evolution in the space direction, as sketched

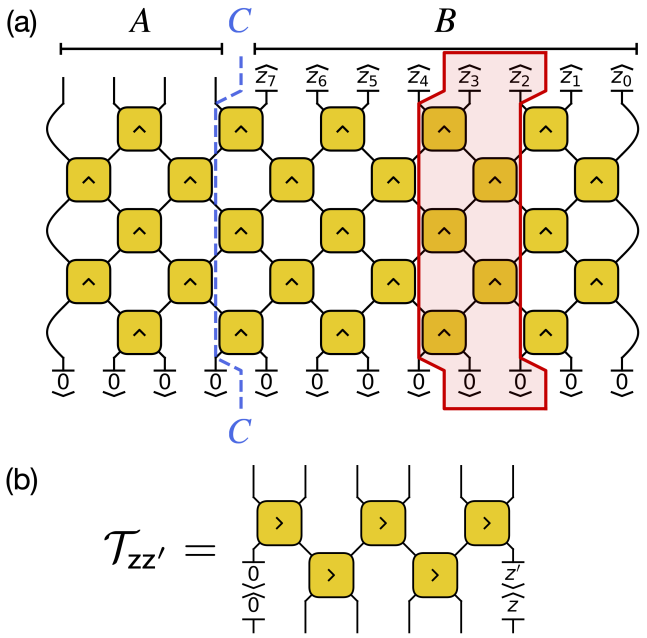

FIG. 2. (a) Setup of the projected ensemble on a one-dimensional brickwork unitary circuit. Yellow squares are two-qubit gates (the arrowhead points in the direction of unitarity); the initial state is a product state $|0\rangle^{\otimes N}$; the final state is projectively measured in B yielding local outcomes $z_i \in \{0, 1\}$ and a pure state in subsystem A (dangling bonds). We also display the time-like subsystem C (dashed line) at the boundary between A and B. In this example, $N_A = 4$, $N_B = 8$, and $t = 5$. (b) Transfer matrix $\mathcal{T}_{zz'}$ that determines the spacetime-dual evolution on C, corresponding to the tensors in the shaded region in (a).

[2] One can straightforwardly define dual-unitary gates on qudits of general dimension [51, 53, 54]; here we focus on qubits for concreteness.

in Fig. 2(a). Each transfer matrix $\mathcal{T}_{zz'}$, sketched in Fig. 2(b), depends on the gates, the initial state, and the final measurements at the corresponding sites (here labeled by bits z, z') that make up the original dynamics. In general, the transfer matrix $\mathcal{T}$ is not unitary, for several reasons. For one, the dualized gates $\tilde{U}$ (represented in Fig. 2(b) by a carat pointing sideways) need not be unitary; secondly, even if the gates are chosen to be dual-unitary, the initial states and the measurements in general break this condition. It is however possible in various models, including the KIM, to find initial states and measurement bases that ensure unitarity of $\mathcal{T}$[9]; we dub these conditions "DU$^+$"[3].

In such a DU$^+$ setting, the dual dynamics is a concatenation of different unitary operators $\mathcal{T}_{zz'}$ labeled by the random measurement outcomes, i.e., a random quantum circuit evolution, beginning from the initial state provided by the open boundary condition to the right. Heuristically, the reason why exact designs may be produced by the projected ensemble on A in this situation is that a product of many random unitaries is generically expected to eventually cover the entire unitary group in the limit of large depth (which corresponds to infinitely many measurements of a large bath). Thus, the distribution of states on the time-like cut C (see Fig. 2(a)) will be uniformly (i.e., Haar) random. Then, by using dual-unitarity, the states on A also acquire a Haar distribution provided $|A| \leq |C|$, as the map going from the time-like cut C to the local subregion A is an isometry, and the projection of a Haar-random state from a higher-dimensional space to a lower-dimensional space is still Haar-random. This fact was shown in Ref. [8] specifically for the KIM, but the result relies only on dual-unitarity and thus is immediately generalizable.

Of course, the subtle point is proving that the random quantum circuit evolutions indeed cover the unitary group, or equivalently, that the unitary transfer matrices $\{\mathcal{T}_{zz'}\}$ constitute a *universal "gate" set* from the point of view of quantum computation. Ref. [8] does so explicitly for the KIM. In Sec. III, we will prove that this is, in fact, almost always the case for spatiotemporally-random DU$^+$ circuits.

C. Monitored dynamics and dynamical purification

Once the DU$^+$ conditions are violated (by choosing gates outside $\mathfrak{DU}$ and/or incompatible initial states and measurement bases), the transfer matrices $\mathcal{T}$ become non-unitary. Thus the reasoning employed in Ref. [8] to derive exact state designs ceases to apply, and it becomes possible to have a separation between distinct design times, i.e., $t_1 < t_k$ for $k > 1$ (where the t_k's are now defined in the ϵ-approximate sense, as in Eq. (16)).

The non-unitary transfer matrices $\mathcal{T}_{zz'}$ can be usefully interpreted as quantum trajectories in a *monitored* evolution [36–38], wherein unitary gates coexist with post-selected (weak or projective) measurements. In this context the monitoring may arise from two distinct mechanisms:

(i) The gates. Given a unitary U, the space-time dual operation $\tilde{U}$ is generically *not* unitary; it can be written as $\tilde{U} = 2MV$, where V is unitary and M is a positive matrix that describes a quantum measurement on two qubits[4] with a fixed outcome. If $U \in \mathfrak{DU}$ then the measurement is trivial, $M \propto \mathbb{I}$.

(ii) The initial state and final measurement basis. In the example of Fig. 2(a) we show the simplest case of an initial state and final measurement in the computational basis; these, as can be seen in Fig. 2(b), dualize to projective measurements on the edge qubits. Different choices may lead to weak measurements, or to no measurements at all (e.g., a measurement of pairs of qubits in the Bell basis), the scenario we labeled DU$^+$.

Monitored quantum dynamics has received significant attention in recent years as a new paradigm for non-equilibrium phase structure [11–15, 55–70]. In particular, starting from a mixed initial state $\rho(0)$, e.g. the fully-mixed state $\rho(0) = \mathbb{I}/2^N$, the ensemble of quantum trajectories $\rho_{\mathbf{m}}(t)$ (where $\mathbf{m}$ here labels the measurement record extracted over the course of the dynamics up to time t) may realize *purification phases* distinguished by the scaling of mixed-state entropy, or purity, of the system[11].

Heuristically, under strong/frequent local measurements, entanglement is destroyed and the states $\rho_{\mathbf{m}}(t)$ quickly become pure: $\rho_{\mathbf{m}} \approx |\psi_{\mathbf{m}}\rangle\langle\psi_{\mathbf{m}}|$, and thus $S(\rho_{\mathbf{m}}(t)) \approx 0$, where S is a measure of entropy, e.g., a Rényi entropy. On the other hand, for sufficiently weak/infrequent measurements, the dynamics manages to protect an extensive, or "volume-law", amount of entanglement, $S(\rho_{\mathbf{m}}(t)) \sim N$, for a long time. These two behaviors are in fact genuine phases, separated by a sharp transition at a critical measurement strength/rate. More precisely, one may define a 'purification time' τ_p as the minimum t such that $\mathbb{E}_{\mathbf{m}}[S(\rho_{\mathbf{m}}(t))] < \epsilon$, for some arbitrary small threshold $\epsilon > 0$; the purification phases are then sharply distinguished in the infinite-system limit by the scaling of τ_p with N, namely $\lim_{N\to\infty} \tau_p(N)/N$ is 0 in the "pure phase" and ∞ in the "mixed phase".

The existence of the mixed phase, and its stability to a finite rate of measurement for an exponentially long time, is particularly surprising. To develop intuition about this

[3] Ref. [9] introduces a related notion of "solvable measurement scheme" based on the spectrum of the transfer matrix; our notion of DU$^+$ implies that notion.

[4] Formally, it is an entry in a POVM set, e.g. $\{M, \sqrt{\mathbb{I} - M^\dagger M}\}$

phase, it is helpful to consider the case of random circuits, where a powerful mapping to statistical mechanics emerges [23, 71, 72]. The problem of dynamical purification in 1+1 dimension maps onto the statistical mechanics of a classical magnet on an $N \times T$ strip, with open boundary conditions at $x = 0, N$ and polarized boundary conditions at $t = 0$ and $t = T$ [67]. The mixed-state entropy $S(N, T)$ is the free energy cost of flipping the boundary polarization at $t = T$ from $\uparrow$ to $\downarrow$, while the polarization at $t = 0$ is fixed to $\uparrow$. The pure phase corresponds to a *disordered* (paramagnetic) phase where correlations are short-ranged; this free-energy cost is thus small, giving low entropy and a nearly-pure state. Conversely, the mixed phase corresponds to an *ordered* (ferromagnetic) phase, where the boundary conditions seed polarized domains that extend into the bulk. For sufficiently small T, the free energy cost is dominated by configurations with a single domain wall between domains of $\uparrow$ and $\downarrow$ spins, $S(N, T) \approx \beta\sigma N - \ln(T)$; here $\beta\sigma$ is a domain-wall line tension and $\ln(T)$ is the entropy term associated to the multiplicity of locations for the domain wall. Thus $S(N, T) \approx \ln(\tau_p/T)$, and we recover an exponential scaling of the purification time $\tau_p \sim e^{\beta\sigma N}$. Finally, for $T \gg \tau_p$ the system reduces to a 1D Ising model and the scaling of entropy is expected to cross over to e^{-2T/τ_p} [67].

Notably, these purification phases are invisible to the first moment of the ensemble of trajectories, $\rho^{(1)} = \sum_{\mathbf{m}} p_{\mathbf{m}} \rho_{\mathbf{m}}$: this linear statistical mixture of the trajectories corresponds to a quantum channel acting on the input state $\rho(0)$; as such, the purity of $\rho^{(1)}$ is bounded above by that of $\rho(0)$, and thus the state remains mixed in both phases. On the contrary, an order parameter that distinguishes the phases is e.g. the trajectory-averaged purity,

$$\sum_{\mathbf{m}} p_{\mathbf{m}} \operatorname{Tr}\left(\rho_{\mathbf{m}}^2\right) = \operatorname{Tr}\left(\rho^{(2)}\chi\right) , \tag{18}$$

which in the r.h.s. we write as the expectation of an observable (χ, a swap between the two replicas of the system) on the second moment $\rho^{(2)}$ of the ensemble $\mathcal{E} = \{p_{\mathbf{m}}, \rho_{\mathbf{m}}\}$. Thus dynamical purification phases in monitored systems probe features beyond regular thermalization that are captured by higher moments of an ensemble, much like the emergence of state designs in the projected ensemble. As we will see in Sec. IV, this connection can be made precise, and our understanding of monitored dynamics can be leveraged to obtain new results on the emergence of state designs in the projected ensemble.

III. EXACT DESIGNS IN DUAL-UNITARY CIRCUITS

In this section, we present our first main result, that random DU^+ circuits (as defined in Sec. II B), which lack dynamical purification physics in their space-time duals, generically achieve an exact quantum state k-design for all k at the thermalization time $t_1 = N_A$. This happens in the limit of infinitely large bath size $N_B \to \infty$. We note of course that there are specific instances of DU^+ circuits that do not exhibit this behavior, e.g. circuits composed of SWAP gates, which are in $\mathfrak{DU}$ but do not generate entanglement, or the KIM at its dual-unitary but integrable point. However, what we show is that *almost all* DU^+ circuits do so, greatly extending the scope of the results of Ref. [8], and showing that the phenomenology of emergent quantum state-designs in dynamics is generic, as far as this class of models goes.

A. Setup and assumptions

Concretely, we consider brickwork circuits made of gates in $\mathfrak{DU}$, with initial states and measurement bases chosen to ensure the unitarity of the transfer matrix $\mathcal{T}$. In particular, we fix an initial state composed of Bell pairs[5], $|\psi_{\text{init}}\rangle = \left|\Phi^0\right\rangle^{\otimes N/2}$, with $\left|\Phi^0\right\rangle \equiv \frac{1}{\sqrt{2}}(|00\rangle + |11\rangle)$ and $N = N_A + N_B$ is the total number of qubits in the system, partitioned into subsystems A and B. While we focus on this initial state for simplicity, any "solvable" matrix-product states (as defined in Ref. [50]) are amenable to the same treatment [9]. We also perform final measurements in the basis of two-qubit Bell states, i.e., pairs of neighboring qubits (that have *not* been coupled by the latest layer of unitary gates) are projectively measured in the orthonormal basis of Bell states $|\Phi^\alpha\rangle \equiv (\sigma^\alpha \otimes \mathbb{I})\left|\Phi^0\right\rangle$. This choice of initial state and final measurement basis is in DU^+, i.e. it guarantees that the transfer matrices $\mathcal{T}_\alpha$ (labeled by the possible outcomes $\alpha = 0, x, y, z$) are unitary. In fact, as shown diagrammatically in Fig. 3(a), such measurements dualize to single-qubit Pauli unitaries, giving

$$\mathcal{T}_\alpha = \mathcal{T}_0 \sigma_t^\alpha, \tag{19}$$

where $\{\sigma_t^\alpha\}$ are the Pauli matrices on site t in the dual system. This is depicted schematically in Fig. 3(b). Note that we define t as the circuit depth (i.e., the number of gates acting on each qubit), so that the size of C is $|C| = t + 1$; we number sites in C as $\{0, 1, \dots t\}$.

We will further consider circuits that are formed by sampling local gates U independently and identically from $\mathfrak{DU}$ according to a probability distribution P. We also require that the distribution P has nonzero weight on an open subset $G \subset \mathfrak{DU}$, as sketched in Fig. 3(c). We impose no other requirements on G; in particular, it can be an arbitrarily small neighborhood of any $V \in \mathfrak{DU}$. For future convenience, we introduce the a notion of "circuit instance" as follows.

---

[5] This partition into pairs requires N to be even; if N is odd, we define $|\psi_{\text{init}}\rangle = \left|\Phi^0\right\rangle^{\otimes \lfloor N/2 \rfloor} \otimes |0\rangle$ instead.

Definition. *A "circuit instance" (or just "instance") is a brickwork quantum circuit in 1+1 dimensions constructed by sampling two-qubit gates independently and identically from a probability distribution P on $\mathfrak{DU}$. The quantum circuit has finite depth t and is semi-infinite in space.*

Given an instance, we may truncate it at a finite length N_B, leaving dangling legs that define the timelike surface C, as in Fig. 3(b), and investigate the statistics of the quantum states produced at C from the dual evolution as N_B is increased. As explained in Sec. II B, it suffices to prove that these states are uniformly distributed, i.e. form a state-design themselves, in order to show that the states comprising the projected ensemble on A are also uniformly distributed (albeit on a different Hilbert space), provided that $|A| \leq |C|$. Below we focus on this situation, i.e. $N_A \leq t+1$. For simplicity, we also assume that $N_A + t$ is odd in the following[6]; the opposite case can be addressed with minor modifications.

B. Spacetime-dual evolution

We define the ensemble of quantum states produced on C, with each state occuring with equal probability, as[7] $\rho^{(k)}$. By exchanging the roles of space and time, we can interpret the state $\rho^{(k)}$ as the output of a quantum channel acting on k "replicas" of system C. This is shown diagrammatically in Fig. 3(d). The channel is given by $\rho \mapsto \frac{1}{4}\sum_\alpha \mathcal{T}_\alpha^{\otimes k}\rho(\mathcal{T}_\alpha^{\otimes k})^\dagger$ By using Eq. (19), we can write the channel as $\rho \mapsto \mathcal{U}^{\otimes k} \circ \mathcal{D}[\rho]$, where $\mathcal{U}$ is a unitary channel acting on a single replica as conjugation by $\mathcal{T}_0, \mathcal{U}[\rho] = \mathcal{T}_0\rho\mathcal{T}_0^\dagger$, and $\mathcal{D}[\rho] = \frac{1}{4}\sum_\alpha(\sigma_t^\alpha)^{\otimes k}\rho(\sigma_t^\alpha)^{\otimes k}$ is a dissipative quantum channel coupling all replicas at one edge (qubit t), represented by the cylinders in Fig. 3(d). We will label the Kraus operators[8] of this channel as $K_\alpha \equiv (\sigma_t^\alpha)^{\otimes k}$, $\alpha = 0, x, y, z$.

Henceforth we use r to refer to "time" in this dual evolution: $r = 1, \dots N_B$. Note that an iteration of the channel $\mathcal{U}^{\otimes k} \circ \mathcal{D}$ corresponds to $\Delta r = 2$. Letting the initial state imposed by the open boundary condition in the original circuit be $\rho_0^{(k)} \equiv (|\psi_0\rangle\langle\psi_0|)^{\otimes k}$, with $|\psi_0\rangle = \left|\Phi^0\right\rangle^{\otimes \lfloor \frac{t+1}{2} \rfloor} \otimes |0\rangle^{\otimes p}$ ($p \equiv (t+1) \mod 2$), the evolved state at dual-time N_B is given by

$$\rho_{N_B}^{(k)} = \mathcal{U}_{N_B}^{\otimes k} \circ \mathcal{D} \circ \mathcal{U}_{N_B-2}^{\otimes k} \circ \mathcal{D} \circ \cdots \circ \mathcal{U}_2^{\otimes k} \circ \mathcal{D}[\rho_0^{(k)}] \ , \quad (20)$$

where we have made explicit the fact that $\mathcal{U}$ depends on r (via the sampling of i.i.d. random gates from $G \subset \mathfrak{DU}$). Our goal now is to characterize the steady state of this sequence of channels: if it is the Haar moment $\rho_H^{(k)}$, we obtain an exact state k-design at C, and thus at A.

We may rewrite Eq. (20) by evolving the Kraus operators in the Heisenberg picture, $K_\alpha(r) \equiv \mathcal{U}_{r\leftarrow 0}^{\otimes k}[K_\alpha]$, where $\mathcal{U}_{r\leftarrow 0} \equiv \mathcal{U}_r \circ \mathcal{U}_{r-2} \circ \cdots \circ \mathcal{U}_2$ is the unitary channel that implements the evolution between (dual) times 0 and r. Thus we have

$$\rho_{N_B}^{(k)} = \mathcal{U}_{N_B\leftarrow 0}^{\otimes k} \circ \mathcal{D}'_{N_B-2} \circ \mathcal{D}'_{N_B-4} \circ \cdots \circ \mathcal{D}'_0[\rho_0^{(k)}] \quad (21)$$

$$\mathcal{D}'_r[\rho] = \frac{1}{4}\sum_\alpha K_\alpha(r)\rho K_\alpha^\dagger(r) \ . \quad (22)$$

As the Haar moment $\rho_H^{(k)}$ is invariant under tensor-product unitaries, we may safely drop the unitary channel $\mathcal{U}_{N_B\leftarrow 0}^{\otimes k}$ and focus on the dissipative part, given by composition of the r-dependent $\mathcal{D}'_r$ channels.

C. Convergence to the Haar moment

In order to prove the emergence of exact state designs, we aim to show that (as $N_B \to \infty$) permutation operators are almost always the unique fixed points of this composition of channels [8, 9]. The outline of the proof is as follows: first, we show that every instance has a limit state $\rho_\infty^{(k)}$ (Appendix B); then, we show $\rho_\infty^{(k)}$ must commute with the time-evolved Kraus operators of $\mathcal{D}$, $K_\alpha = (\sigma_t^\alpha)^{\otimes k}$; finally, we show that products of these time-evolved K_α operators generate the group $U(d_C)^{\otimes k} \equiv \{V^{\otimes k} : V \in U(d_C)\}$ *almost surely*, i.e., with probability that approaches 1 as $N_B \to \infty$. (Here $d_C = 2^{|C|} = 2^{t+1}$ is the Hilbert space dimension of C.) From this, the formation of exact designs follows precisely from the same argument as in Ref. [8].

Theorem. *The limit state $\rho_\infty^{(k)}$ is almost always the Haar moment $\rho_H^{(k)}$.*

Before proceeding to the proof, let us stress that the above result does not refer to the ensemble-averaged behavior of the random brickwork circuits; crucially, it holds at the level of a given circuit instance.

Proof. We bound the commutators between $\rho_\infty^{(k)}$ and the Kraus operators $\{K_\alpha(r)\}$ by triangle inequality,

$$\begin{aligned}\|[\rho_\infty^{(k)}, K_\alpha(r)]\| &\leq \|[\rho_\infty^{(k)} - \rho_r^{(k)}, K_\alpha(r)]\| + \|[\rho_r^{(k)}, K_\alpha(r)]\| \\ &\leq 2\|\rho_\infty^{(k)} - \rho_r^{(k)}\| + \|[\rho_r^{(k)}, K_\alpha(r)]\| \ , \quad (23)\end{aligned}$$

where $\|\cdots\|$ is the trace norm and we used $\|AB\| \leq \|A\|_\infty\|B\|$ and $\|K_\alpha(r)\|_\infty = 1$. By definition of limit state, there exists $r^*(\epsilon)$ such that for all $r > r^*(\epsilon)$ the first term is $\leq \epsilon$. The second term is also $\leq \epsilon$ due to a Lemma proven in Appendix B. Thus the limit state must commute, up to arbitrary accuracy ϵ, with an infinite sequence of Heisenberg-evolved operators $\{K_\alpha(r) :$

---

[6] This ensures that Bell measurements of B can be performed without leaving an unpaired qubit near the the boundary between A and B.

[7] Note that we have previously used this notation for the state produced at A; however, for the rest of this Section, we will focus uniquely on the state produced at C, so that there will be no ambiguity.

[8] Note that we choose to leave the prefactor 1/2 outside the definition of K_α for future convenience. Therefore, the operators obey a modified normalization condition $\sum_\alpha K_\alpha^\dagger K_\alpha = 4\mathbb{I}$.

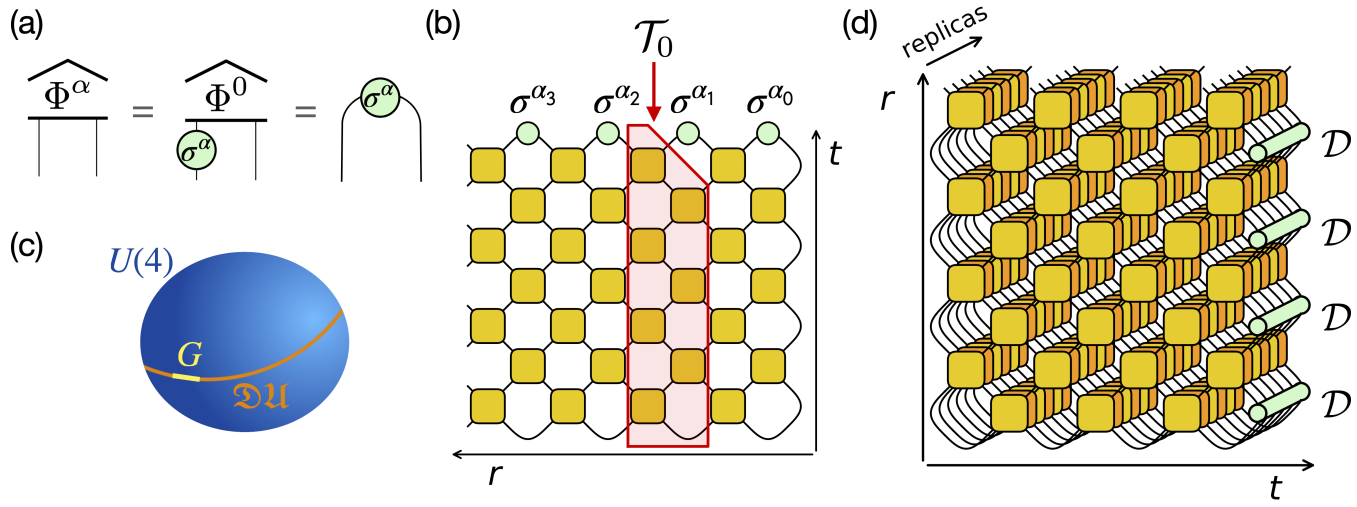

FIG. 3. Emergence of exact state designs in random DU$^+$ circuits. (a) Projection onto the Bell state $|\Phi^\alpha\rangle$ is space-time dual to a single-qubit Pauli unitary σ^α. (b) Instance of a random dual-unitary circuit of depth $t = 7$, truncated in the space direction at $N_B = 8$. Squares represent dual-unitary gates, circles represent Pauli unitaries obtained from the Bell measurements. The shaded area represents a (unitary) transfer matrix $\mathcal{T}_0$. (c) Schematic of $U(4)$ (the unitary group on two qubits), $\mathfrak{DU}$ (the submanifold of dual-unitary gates), and G (an open subset of $\mathfrak{DU}$ where the gates making up each circuit instance may be sampled from). (d) Tensor network diagram for the state $\rho^{(k)}$ at C, for $k = 3$, under space-time duality. The diagram is a stack of k replicas of the unitary circuit (lighter gates) and k replicas of its adjoint (darker gates). The average over measurement outcomes couples the replicas at an edge via a quantum channel $\mathcal{D}$ (green cylinders) repeatedly over dual-time r.

$r > r^*(\epsilon)\}$. In Appendix C, we show that, in almost all circuit instances, the set $\{\mathcal{U}_{r\leftarrow 0} : r \in 2\mathbb{N}\}$ is dense in the space of unitary channels (the proof proceeds by showing any open set $G \subset \mathfrak{DU}$ is a universal gate set in the quantum computing sense [10]). Thus for any site $j \in \{0, \dots t\}$ and any two unit vectors $\mathbf{n}_{1,2}$ in S^2, there almost surely exist $r^*_{1,2}$ such that $\sigma^z_t(r^*_{1,2}) = \mathbf{n}_{1,2} \cdot \boldsymbol{\sigma}_j$ up to arbitrary accuracy $\epsilon > 0$. The limit state $\rho^{(k)}_\infty$ must therefore commute (almost always, up to accuracy ϵ) with the product $K_z(r^*_1)K_z(r^*_2) = \exp(i\theta \mathbf{n}_3 \cdot \boldsymbol{\sigma}_j)^{\otimes k}$. The angle θ and direction $\mathbf{n}_3$ can be made arbitrary by choosing $\mathbf{n}_{1,2}$, thus generating the k-fold tensor powers of all single-qubit unitaries. The same reasoning can be applied for entangling operations between any two qubits: for example there almost always exists r^* such that $\sigma^z_t(r^*) \simeq e^{-i\theta\sigma^x_i\sigma^x_j}\sigma^z_i e^{i\theta\sigma^x_i\sigma^x_j}$, which is an entangling operation between qubits i and j. Thus the limit state almost always commutes with a set of operators that generate the entire group $U(d_C)^{\otimes k}$. As the only operators that satisfy this condition exactly are permutations between the replicas (this follows from a mathematical result called the Schur-Weyl duality [18, 73]), and the initial state $\rho^{(k)}_0$ is permutation-symmetric, we conclude that almost surely $\rho^{(k)}_\infty \propto \sum_{\pi\in S_k} \hat{\pi}$, where $\hat{\pi}$ is the operator on $\mathcal{H}_C^{\otimes k}$ that permutes replicas according to an element of the symmetric group $\pi \in S_k$; upon imposing unit trace, we conclude $\rho^{(k)} = \rho^{(k)}_H$ almost always. ■

We note that the result is independent of the gate set $G \subset \mathfrak{DU}$, provided this is an open subset. So we are free to take G as a ball of radius W around any dual-unitary gate $U \in \mathfrak{DU}$, take the limit $N_B \to \infty$ to recover the exact state designs at C (and thus at A, following the discussion in Sec. II B), and then make W arbitrarily small, similar to the derivation of the spectral form factor in Ref. [52]. In other words, this result applies to arbitrary dual-unitary circuits with arbitrarily weak, spatiotemporally-uncorrelated disorder.

IV. AWAY FROM DUAL-UNITARITY: CONSTRAINTS FROM DYNAMICAL PURIFICATION

As soon as we break the DU$^+$ conditions, either by perturbing the gates away from dual-unitarity or by modifying the initial state or final measurement basis, the above derivation fails. The transfer matrices become non-unitary, and the physics of monitored dynamics, reviewed in Sec. II C, comes into play. In this Section we derive the consequences of this fact on the k-design times t_k.

A. Bounding the purity of the k-th moment

The connection to monitored dynamics is sharpened in the following, which is one of the main results of this work.

Theorem. *Consider a projected ensemble* $\{(p(\mathbf{z}_1, \mathbf{z}_2), |\psi_{\mathbf{z}_1,\mathbf{z}_2}\rangle)\}$ *on a system of size* N*, where the projected states and probabilities are indexed by*

the bit-string $(\mathbf{z}_1, \mathbf{z}_2)$ *such that* $\mathbf{z}_1 \in \{0,1\}^r$ *and* $\mathbf{z}_2 \in \{0,1\}^{N-r}$ *for some integer* $r \geq 0$. *Then, we have*

$$\mathrm{Tr}\left(\rho^{(k)^2}\right) \geq \frac{1}{2^r}\left(\mathbb{E}_{\mathbf{z}_1}\,\mathrm{Tr}\left[(\rho^{(1)}_{\mathbf{z}_1})^2\right]\right)^k, \tag{24}$$

where $\rho^{(1)}_{\mathbf{z}_1} = \sum_{\mathbf{z}_2} p(\mathbf{z}_2|\mathbf{z}_1)\,|\psi_{\mathbf{z}_1,\mathbf{z}_2}\rangle\langle\psi_{\mathbf{z}_1,\mathbf{z}_2}|$ *is a density matrix defined in terms of the conditional probabilities* $p(\mathbf{z}_2|\mathbf{z}_1) = p(\mathbf{z}_2,\mathbf{z}_1)/p(\mathbf{z}_1)$ and $\mathbb{E}_{\mathbf{z}_1}[\cdot] = \sum_{\mathbf{z}_1} p(\mathbf{z}_1)[\cdot]$.

Proof. We may write the l.h.s. as

$$\begin{aligned}\mathrm{Tr}\left(\rho^{(k)^2}\right) &= \sum_{\mathbf{z}_1,\mathbf{z}_1'} p(\mathbf{z}_1)p(\mathbf{z}_1') \sum_{\mathbf{z}_2,\mathbf{z}_2'} p(\mathbf{z}_2|\mathbf{z}_1)p(\mathbf{z}_2'|\mathbf{z}_1') \\ &\quad\times \left|\langle\psi_{\mathbf{z}_1,\mathbf{z}_2}|\,\psi_{\mathbf{z}_1',\mathbf{z}_2'}\rangle\right|^{2k} \\ &= \sum_{\mathbf{z}_1,\mathbf{z}_1'} p(\mathbf{z}_1)p(\mathbf{z}_1')\,\mathrm{Tr}\left(\rho^{(k)}_{\mathbf{z}_1}\rho^{(k)}_{\mathbf{z}_1'}\right)\end{aligned} \tag{25}$$

in terms of the k-th moments of the conditional ensembles. Then, by noting that all terms in the sum are non-negative and dropping off-diagonal terms, we have the inequality:

$$\mathrm{Tr}\left(\rho^{(k)^2}\right) \geq \sum_{\mathbf{z}_1} p(\mathbf{z}_1)^2\,\mathrm{Tr}\left[(\rho^{(k)}_{\mathbf{z}_1})^2\right]. \tag{26}$$

At this point, we make use of two inequalties proven in Appendix D: first, for any ensemble $\mathcal{E}$ we have the following bound between the purities of the first and k-th moment,

$$\mathrm{Tr}\left(\rho^{(k)^2}\right) \geq \left[\mathrm{Tr}\left(\rho^{(1)^2}\right)\right]^k; \tag{27}$$

second, given a probability distribution $p(i)$ over M elements and a non-negative function $f(i)$, we have

$$\sum_i p(i)^2 f(i)^k \geq \frac{1}{M}\left(\sum_i p(i)f(i)\right)^k. \tag{28}$$

Now, returning to Eq. (26), we have

$$\begin{aligned}\mathrm{Tr}\left(\rho^{(k)^2}\right) &\geq \sum_{\mathbf{z}_1} p(\mathbf{z}_1)^2\left[\mathrm{Tr}\left(\rho^{(1)^2}_{\mathbf{z}_1}\right)\right]^k \\ &\geq \frac{1}{2^r}\left(\sum_{\mathbf{z}_1} p(\mathbf{z}_1)\,\mathrm{Tr}\left(\rho^{(1)^2}_{\mathbf{z}_1}\right)\right)^k,\end{aligned} \tag{29}$$

where the first line follows from Eq. (27) and the second line follows from applying Eq. (28) to the probability distribution $p(\mathbf{z}_1)$ (over $M = 2^r$ elements) and the function $f(\mathbf{z}_1) = \mathrm{Tr}\left(\rho^{(1)^2}_{\mathbf{z}_1}\right)$. ■

The result Eq. (24) places a constraint of the formation of state designs. Indeed, as we saw in Sec. II A, the l.h.s. equals the frame potential $F^{(k)}$ of the ensemble, which in turn can be used to formulate the k-design condition: one has $F^{(k)} \geq F^{(k)}_H \equiv \binom{2^{N_A}+k-1}{k}^{-1}$, with equality if and only if $\mathcal{E}$ forms a k-design. If the ensemble $\mathcal{E}$ is to form a k-design, then the r.h.s. must not exceed the Haar frame potential $F^{(k)}_H$.

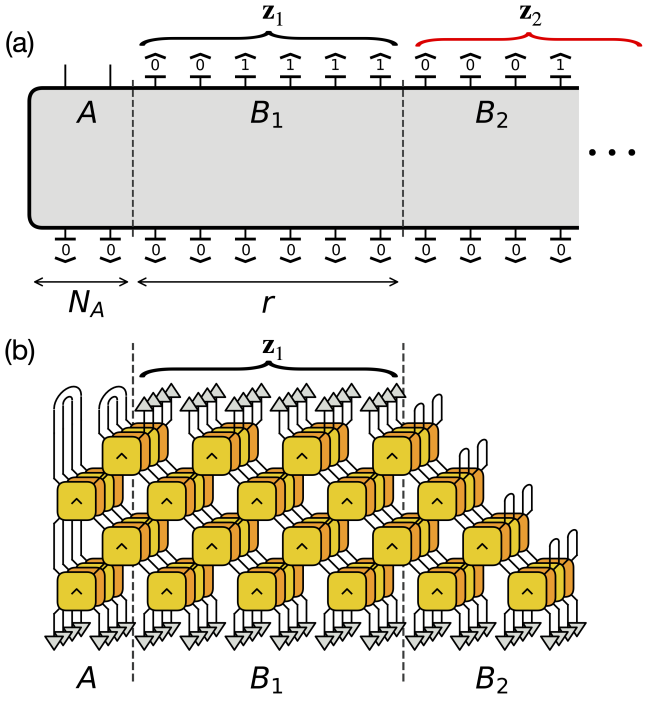

FIG. 4. (a) Setup of Eq. (24): the 'bath' subsystem B is partitioned into sub-regions B_1 (of size r) and B_2, yielding measurement outcomes $\mathbf{z}_1$ and $\mathbf{z}_2$ (example bitstrings are shown). From this setup one may form the conditional ensembles $\{p(\mathbf{z}_2|\mathbf{z}_1), |\psi_{\mathbf{z}_1,\mathbf{z}_2}\rangle\}$ and their first moments $\rho^{(1)}_{\mathbf{z}_1}$. (b) Tensor network diagram for the purity of $\rho^{(1)}_{\mathbf{z}_1}$ (up to a normalization factor $p(\mathbf{z}_1)^2$). Note the different contractions within subsystems A and B_2. Due to unitarity, all but the nearest t qubits in B_2 are elided. Viewed as an evolution in the space direction (from right to left), the diagram describes the dynamical purification of an initially mixed state.

B. Monitored dynamics and purification

In the case of one-dimensional quench dynamics, the r.h.s. of Eq. (24) lends itself naturally to an interpretation in the language of monitored dynamics (reviewed in Sec. II C). Let us consider a one-dimensional qubit chain partitioned into a finite subsystem A (comprising the leftmost N_A qubits) and its complement B, which serves as the bath to be measured in order to form the projected ensemble on A. In addition, we split B into two subsystems, B_1 comprising the r qubits closest to A, and the remainder B_2, as illustrated in Fig. 4(a). We may then apply Eq. (24) to this situation to bound the purify of the k-th moment of the projected ensemble, with $\mathbf{z}_1 \equiv \mathbf{z}_{B_1}$ and $\mathbf{z}_2 \equiv \mathbf{z}_{B_2}$.

The term in the parenthesis of the r.h.s. of Eq. (24) yields a setup that has a direct interpretation in the language of monitored dynamics. Specifically, the quantity

$$\mathbb{E}_{\mathbf{z}_1}\,\mathrm{Tr}\left[(\rho^{(1)}_{\mathbf{z}_1})^2\right] \tag{30}$$

is the purity of the density matrix $\rho^{(1)}_{\mathbf{z}_1}$, shown diagram-

matically in Fig. 4(b), ensemble-averaged over measurement outcomes $\mathbf{z}_1$. What $\rho^{(1)}_{\mathbf{z}_1}$ in turn represents, upon invoking a space-time duality transformation, is an initially *highly-mixed* density matrix $\rho_{\rm in}$ on a system of $|C| = t+1$ qubits (since the B_2 region is being traced out, as shown as the right boundary condition of Fig. 4(b)) undergoing a quantum circuit evolution indexed by $\mathbf{z}_1 \in \{0,1\}^r$ in region B_1, before being mapped to A. As reviewed in Sec. II C, this quantum circuit can be segmented into transfer matrices, which are generically non-unitary and can be viewed as trajectories in a monitored evolution. In total, the depth of this monitored evolution is r. This is an instance of the problem of *dynamical purification* of mixed states [11]. Ref. [37] showed that space-time duals of unitary circuits are generically in the *mixed phase* of the dynamical purification problem, where for a system of N qubits one has $\tau_p \sim \exp(N)$ [11, 61, 67].

Thus, by interpreting the r.h.s. of Eq. (24) as a spacetime-dual purification dynamics, we can write it as $2^{-r-kS_2^{(a)}(r)}$, where $S_2^{(a)}$ is the "annealed average" of the second Rényi entropies of the ensemble states (measured in bits), i.e., $S_2^{(a)} = -\log_2 \mathbb{E}_{\mathbf{z}_1} \operatorname{Tr}\left[(\rho^{(1)}_{\mathbf{z}_1})^2\right]$. In the following we simply denote this quantity by S, and we assume the scaling argued in Sec. II C, $S(r) \sim e^{-2r/\xi_p}$ at large r, where ξ_p is a "purification length scale" that diverges exponentially in t (in analogy with τ_p vs N in our previous discussion). We also define a *purification velocity*

$$v_p \equiv \lim_{t\to\infty} \frac{1}{t} \log_2 \xi_p(t) \,, \tag{31}$$

playing the role of the domain wall line tension $\beta\sigma$ in the discussion of Sec. II C.

C. Constraints on the design times

To recapitulate, Eq. (24) relates the formation of state designs (represented by the frame potential $F^{(k)}$ in the l.h.s.) to the problem of dynamical purification in the spacetime-dual dynamics (represented by the r-dependent average purity in the r.h.s.). This allows us to derive constraints on the formation of state designs by using insights about dynamical purification. Heuristically, the finite memory time of monitored dynamics may cause measurement outcomes very far away from A to be "forgotten" and thus effectively limit the size of the projected ensemble, which obstructs the formation of high designs. This is in contrast to DU^+ circuits, where the dual evolution is unitary and thus has perfect memory – measurement outcomes arbitrarily far away always have an effect on the state in A.

Concretely, we may rewrite Eq. (24) as

$$\ln\left(1/F^{(k)}\right) \le \ln(2)[r + kS(r)] \,. \tag{32}$$

This is a family of bounds parametrized by $r \in \mathbb{N}$, all of which must be satisfied. We can replace this family of bounds by the most stringent one, i.e. minimize the r.h.s. over r. This yields $r = r^*(k)$, where r^* solves[9] $S'(r^*) = -1/k$. Here we invoke our ansatz motivated by dynamical purification: we assume $S(r)$ monotonically decreases and asymptotes to 0. This implies that its derivative $S'(r) < 0$ also asymptotes to 0, so $r^*(k)$ diverges as $k \to \infty$. This ensures that, if we take k large enough, r^* lies in the domain of applicability of the large-r ansatz $S(r) \sim e^{-2r/\xi_p}$. Minimizing the r.h.s. under this ansatz gives $r^* = \frac{\xi_p}{2} \ln \frac{2k}{\xi_p}$, and thus the bound

$$\ln\left(1/F^{(k)}\right) \le \xi_p \frac{\ln(2)}{2} \ln\left(\frac{2ek}{\xi_p}\right) \,. \tag{33}$$

The ϵ-approximate k-design condition $\Delta_2^{(k)} \le \epsilon$ (see Eq. (16)) yields $F^{(k)} \le (1+\epsilon^2) F_H^{(k)}$, where $F_H^{(k)} \equiv \binom{2^{N_A}+k-1}{k}^{-1}$ is the frame potential of the Haar ensemble, as in Eq. (15). Thus

$$\ln\binom{2^{N_A}+k-1}{k} - \ln\left(1+\epsilon^2\right) \le \xi_p \frac{\ln(2)}{2} \ln\left(\frac{2ek}{\xi_p}\right) \,. \tag{34}$$

We may now take $k \to \infty$ (which is consistent with the regime of applicability of our ansatz for $S(r)$). In this limit, using $\ln\binom{k+n}{k} = n\ln(k) - \ln(n!) + O(1/k)$ we have that both sides of Eq. (34) diverge as $\ln(k)$; thus we obtain a bound on the prefactors of $\ln(k)$,

$$2^{N_A} - 1 \le \xi_p(t) \frac{\ln(2)}{2} \,. \tag{35}$$

This bound holds for any value of N_A, and constrains the time needed to form infinitely high designs, $t_\infty \equiv \lim_{k\to\infty} t_k$. Finally, for large t and N_A, Eq. (35) reduces to

$$t_\infty \ge \frac{N_A}{v_p} \,. \tag{36}$$

In the same limit (large N_A), the thermalization time t_1 defines the "entanglement velocity", $v_E \equiv N_A/t_1$. Using this definition to eliminate N_A yields the inequality

$$t_\infty \ge \frac{v_E}{v_p} t_1 \,, \tag{37}$$

which is another main result of our work.

Eq. (37) shows that, whenever $v_p < v_E$, we have a guaranteed minimum separation between t_1 (governing the formation of a 1-design, or regular thermalization) and t_∞ (governing the formation of high designs, or "deep" thermalization).

[9] We make r continuous and interpolate $S(r)$ to a smooth function of a real variable.

D. Tuning the purification velocity

As $t_\infty \geq t_1$ is always true, in order for Eq. (37) to be nontrivial, one must be able to tune v_p below v_E. Here we discuss some examples in which this can be achieved, displaying a genuine separation between design times.

We consider DU circuits with solvable initial states, where it is known that $v_E = 1$ [50]. By choosing the gates and the final measurement basis, it is possible to vary v_p significantly while v_E is pinned to 1. Evidence of this can be seen by simulating random DU circuits with variable gate sets and measurement bases. In particular, we consider measurement bases that interpolate smoothly between the Bell basis and the computational basis, parametrized by $\mu \in [0, 1]$. Specifically, we project pairs of qubits onto pure states $|\psi^a_\mu\rangle \propto (I \pm \mu\sigma^z_1)\,|\Phi^a\rangle$, where $\{|\Phi^a\rangle : a = 0, x, y, z\}$ is the Bell basis. Note that for $\mu = 0$ we recover exactly the Bell basis, while for $\mu = 1$ we obtain a disentangled basis $\{|00\rangle, |01\rangle, |10\rangle, |11\rangle\}$; the entanglement of the basis states decreases monotonically with μ.

We simulate the spacetime-dual (monitored) dynamics of circuits formed from random DU gates (specifically, the single-qubit gates r, s, u, v are Haar-random in $SU(2)$ and J is uniformly distributed in $[0, \pi/4]$), acting on $t + 2$ qubits, one of which serves as a reference R (i.e., is initially entangled with the rest and is not touched afterwards). As shown in Fig. 5(a), this reproduces the setup of Eq. (24) with a minimal subsystem B_2 (the single reference qubit R), a subsystem B_1 of length r (duration of the dual time evolution), and a subsystem C of $t + 1$ qubits. As a result of the measurements on B_1, the evolution is generally monitored (other than at $\mu = 0$, where we measure B_1 in the Bell basis and thus fulfill the DU$^+$ conditions). The family of measurement bases we introduced above, parametrized by $\mu \in [0, 1]$, dualizes to *weak measurements* on the last system qubit; these are given by Kraus operators $K_\pm \propto I \pm \mu\sigma^z$ followed by single-qubit Pauli gates. Note that for $\mu = 1$ we recover strong σ^z measurements, while for $\mu = 0$ we obtain purely unitary operations.

We compute the entropy $S(r)$ of the reference qubit as a function of r, and observe an exponential decay $S(r) \sim e^{-2r/\xi_p(t)}$ (Fig. 5(b)). The purification length scale $\xi_p(t)$ is found to be consistent with the expected behavior $\sim \exp(t)$ in the numerically explored range, $8 \leq t \leq 18$ (Fig. 5(c)). Moreover, as the "measurement strength" μ is tuned we find a significant variation of the purification velocity v_p, extracted from exponential fits to $\xi_p(t)$. Fig. 5(d) shows that v_p approaches 1 from below as $\mu \to 0$. This is in line with the results of Sec. III: $\mu = 0$ corresponds to the DU$^+$ regime where we have proven the instantaneous emergence of all state designs, i.e. $t_k = t_1 = N_A/v_E$ for all k; this immediately implies that the bound in Eq. (37) must be trivial, i.e. $v_p \geq v_E$. Recalling that in this case $v_E = 1$, we must have $v_p \geq 1$ as $\mu \to 0$. For $\mu \neq 0$, we see $v_p < 1$, indicating a separation between the regular thermalization time and higher state-design formation time.

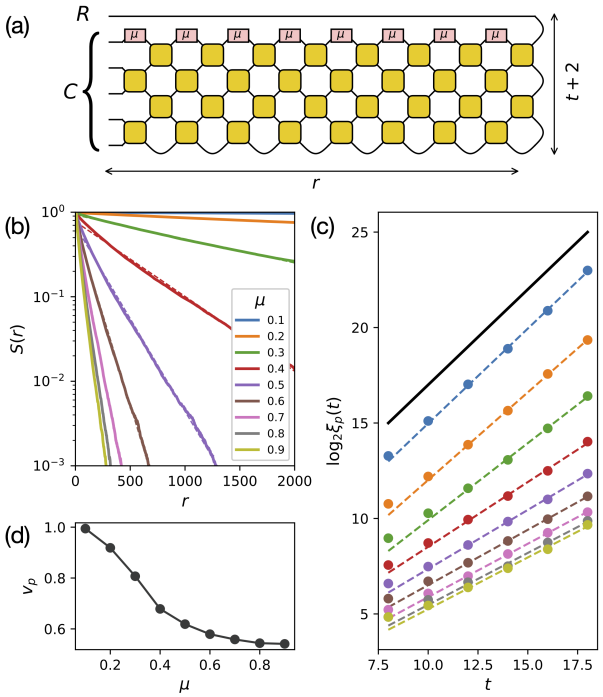

FIG. 5. Tuning the purification velocity v_p in DU circuits. (a) Circuit setup for the numerical simulations: an initial state is prepared on $t + 2$ qubits (right end), with one qubit set aside as a reference R; the remaining $t + 1$ qubits, making up system C, evolve under DU gates (yellows squares) and measurements (boxes labelled by μ) at an edge qubit. This example shows $t = 4$. The entanglement between R and C is computed as a function of dual-time r. (b) Entropy of the reference qubit $S(r)$ for a $t = 12$ and varying measurement scheme μ ($\mu = 0$ gives Bell measurements, $\mu = 1$ gives Z measurements). We use the annealed average of the second Renyi entropy, $S \equiv S^{(a)}_2$, as in Eq. (24). Dashed lines are exponential fits, $S(r) \sim e^{-2r/\xi_p(t)}$. Numerical data is obtained from exact simulations and averaged over between 500 and 10000 realizations, depending on system size. (c) Purification lengthscale $\xi_p(t)$ vs t, extracted from fits as shown in (b). The values of μ are the same and indicated by the same colors. The solid line has unit slope, for reference. The dashed lines are exponential fits $\xi(t) \sim 2^{v_p t}$. (d) Extracted values of v_p vs μ. We observe $v_p \to 1$ as $\mu \to 0$.

In fact, the separation between v_p and v_E, and thus between t_1 and t_∞, can be made arbitrarily large. To this end, we consider random DU circuits with gates sampled from a gate set $G = \{r_1 s_2 \mathsf{SWAP} e^{-iJZ_1Z_2} u_1 v_2 : |J| < \frac{\pi}{4}\mathcal{J}\} \subset \mathfrak{DU}$, where $r, s, u, v \in SU(2)$ are unconstrained and the parameter $\mathcal{J}$ plays the role of an interaction strength. Namely, as $\mathcal{J} \to 0$ we recover non-interacting SWAP circuits, while for $\mathcal{J} = 1$ we have $G = \mathfrak{DU}$. We numerically simulate the same setup considered in Fig. 5, although with fixed $\mu = 1$ (i.e., measurements in the computational basis) and variable $\mathcal{J}$. Results, in Fig. 6, show that v_p approaches 0 as $\mathcal{J} \to 0$. Note that this

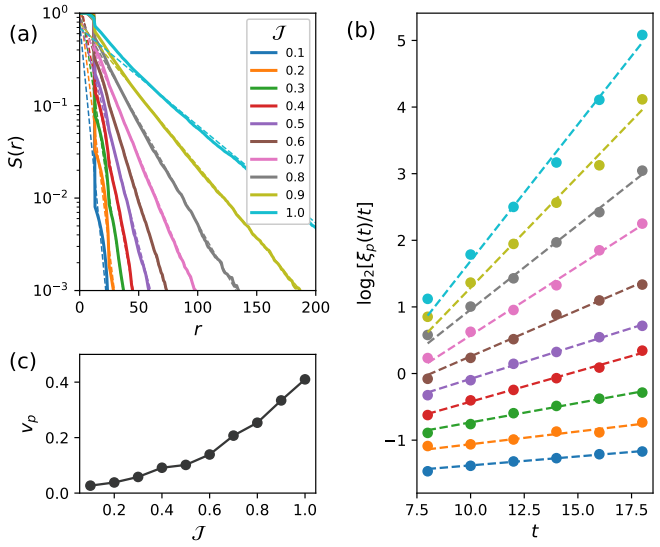

FIG. 6. (a) Same setup as Fig. 5, but for fixed measurement basis (computational basis, corresponding to $\mu = 1$) and variable interaction strength $\mathcal{J}$. Numerical data is obtained from exact simulations and averaged over between 200 and 10000 realizations, depending on system size. (b) Purification length scale $\xi_p(t)$, extracted from fits as shown in (a). The values of $\mathcal{J}$ are the same and indicated by the same colors. We plot the normalized quantity $\xi_p(t)/t$ to eliminate a prefactor of t that arises in the limit of $\mathcal{J} \to 0$. The dashed lines are exponential fits $\xi_p(t)/t \sim 2^{v_p t}$. (c) Extracted values of v_p vs $\mathcal{J}$. We observe $v_p \to 0$ as $\mathcal{J} \to 0$.

limit yields a "critical" purification, $\xi_p \propto t$, owing to the fact that measurements happen only at an edge of the system and qubits must travel (ballistically) to that edge in order to be measured and purified. While this algebraic prefactor does not modify the definition of v_p, it does impact numerical fits on a limited dynamical range when v_p is small; for this reason, we extract v_p from fits to the normalized quantity ξ_p/t, shown in Fig. 6(b).

These numerical results ($0 \leq v_p \leq 1$, with $v_p = 1$ at DU$^+$ and $v_p = 0$ in non-interacting circuits) are in line with expectations from the theory of measurement-induced entanglement transitions, reviewed in Sec. II C. In particular, they are suggestive of the fact that v_p should correspond to a *line tension* in a statistical-mechanical description of entanglement in the random circuit[57, 58, 67, 68]. Universal scaling arguments therein give reason to believe that the same line tension controls both v_p and the polynomial-depth "plateau" of the entropy density (i.e. the order parameter of the mixed phase[11]) during dynamical purification. Since the latter is between 0 and 1 (if we measure the entropy in bits), this correspondence would automatically yield the observed range of v_p. Finally, as one takes the measurement strength to zero one expects the maximum of the entropy density to be achieved, and thus the equality $v_p = 1$; on the contrary, taking the interaction strength to zero achieves the minimum value $v_p = 0$, corresponding to an instability of the mixed phase towards critical purification [36].

V. DISCUSSION

We have analyzed the physics of formation of quantum state designs in the projected ensemble, a novel emergent random matrix universality, arising from states generated under the dynamics of one-dimensional quantum systems, that we modeled by unitary circuits. The formation of state k-designs provides a hierachy of time scales, $\{t_k : k \in \mathbb{N}\}$, that include the thermalization time t_1, but also other scales $t_{k>1}$ whose physical significance is still largely unclear. By connecting this problem to the phenomenology of monitored systems, through a space-time duality approach, we have highlighted the important role of dynamical purification in differentiating the formation of high designs from regular thermalization.

First, we have shown that in the absence of dynamical purification (achieved in a class of models that we named DU$^+$, characterized by dual-unitary gates and compatible initial states and final measurements), one generically obtains *exact* state designs, and all time scales t_k collapse onto the thermalization time t_1. This extends the phenomenology recently discovered in a Floquet Ising model [8] to a wide class of spatiotemporally-disordered models. Secondly, we have shown that, upon breaking the DU$^+$ conditions and restoring dynamical purification, it is possible to derive nontrivial constraints on the design times, in particular a separation between the thermalization time t_1 and the time needed to form ultra-high designs, $t_\infty = \lim_{k\to\infty} t_k$.

The bound we have derived, $t_\infty > (v_E/v_p)t_1$, is nontrivial whenever the "purification velocity" v_p of the circuit is smaller than its "entanglement velocity" v_E. We have shown, with physical arguments corroborated by numerical simulations, that this can be realized in a wide class of models, and that the separation can in fact be made arbitrarily large—e.g. one can take $v_p \to 0$ with constant $v_E = 1$, as shown in Fig. 6. Nonetheless, our bound for t_k is only $O(1)$ in $k \to \infty$. It is an interesting open question whether our bounds are tight; in particular, is it possible to derive (either from dynamical purification arguments or from independent routes) bounds that *diverge* in k? On a discrete set of d elements, a probability distribution only has a finite number of independent moments (namely $d-1$), therefore k-designs beyond $k = d$ are all trivially formed at the same time, and the limit $k \to \infty$ cannot yield divergent time scales. The situation is more nuanced on continuous sets (such as the Hilbert space $\mathcal{H}_A$)[18]; thus it is not clear *a priori* that such a divergent bound, $t_k > f(k)$ for some f obeying $\lim_{k\to\infty} f(k) = \infty$, can be ruled out on general grounds.

As we have shown, the formation of higher state-designs in the projected ensemble probes physics that go beyond regular quantum thermalization. We con-

clude with a set of exciting directions for future research, which aims to better understand the connection between this novel phenomenon and various other aspects of non-equilibrium dynamics:

Scrambling. The models displaying the strongest separation of time scales between t_1 and t_∞ are notably weakly-interacting, suggesting a connection to quantum information scrambling[16–21, 24, 74]. It is thus interesting to sharpen the connection between the formation of high designs and the well-established diagnostics of scrambling, such as out-of-time-ordered correlators [19, 20, 74] and the tripartite mutual information of the circuit [17, 75]. In particular, what is the relationship between the "butterfly velocity" v_B that controls scrambling and the "purification velocity" v_p that governs high designs? While the former is a property of the bulk circuit and of the initial state, the latter is also dependent on a choice of final measurement basis on the "bath"; thus presumably any relationship between the two ought to involve an average or optimization of v_p over the choice of local measurement basis.

Chaos/Ergodicity. There are striking similarities between the derivation of the exact RMT spectral form factor (in the KIM [43] and subsequently in generic DU circuits [52]) and the derivation of exact state designs (also in the KIM [8] and extended to generic DU$^+$ circuits in this work), both of which leverage a space-time duality mapping in order to derive different incarnations of RMT behavior in microscopic models of dynamics. There are also crucial distinctions, however, such as the need for a Floquet evolution in the former and the dependence on initial and final states in the latter. Another important distinction is that in the former, an ensemble average (e.g., over disorder realizations) is required because the spectral form factor is not self-averaging [76], while in the latter, the result appears already at the level of a *single* quantum many-body state. It is intriguing to speculate on a deeper connection between the two phenomena, such as what role quantum chaos might play in the formation of high state designs in the projected ensemble, or even whether the emergence of quantum state designs can be used as an alternative definition of many-body quantum chaos.

Integrability. Models with $v_E > 0$ and $v_p = 0$ thermalize, but fail to form high designs in the projected ensemble. An example of this is a SWAP circuit acting on an initial state of Bell pairs: this model generates entanglement between subsystems by transporting entangled excitations. Interestingly, this can be viewed as a cartoon model of post-quench entanglement generation in integrable models [77, 78]. Does this behavior (thermalization without higher design fomation) generalize to non-trivial, interacting models? Exploring this question in tractable circuit models of interacting-integrable systems [79–81] is an interesting next step.

Teleportation/complexity transition. Lastly, we note that our results apply only to models in one spatial dimension, where the mutual information between two spatially-separated degrees of freedom (upon measuring all the others) decays exponentially with distance. This is at the core of our ansatz for the scaling of entropy $S(r)$ that enables the derivation of our bound between t_1 and t_∞, and is a consequence of the absence of long-range order in one dimension. However, in higher dimension one generically expects a finite-depth transition where said mutual information becomes finite even at infinite distance—a phenomenon that can be interpreted as a *teleportation transition* [82], closely related to a phase transition in the complexity of sampling the output of shallow two-dimensional circuits [83]. An exciting question is how this transition might impact the projected ensemble on states formed from quench dynamics in higher-dimensional systems. For example, can the teleportation/complexity transition be detected by analyzing quantitative features of the formation of high designs? In the "ordered" phase, where our arguments based on dynamical purification cease to apply, is there still generically a separation between the time scales t_1 and t_∞? It is tempting to speculate that the instantaneous formation of all designs after crossing a critical time, which requires the non-generic DU^+ condition in one spatial dimension, might in contrast be generically realized in higher dimensional systems.

ACKNOWLEDGMENTS

We thank S. Choi, T. Rakovszky and V. Khemani for discussions and for previous collaborations on related topics. M. I. is supported by the Gordon and Betty Moore Foundation's grant GBMF8686 and by the Defense Advanced Research Projects Agency (DARPA) via the DRINQS program. The views, opinions and/or findings expressed are those of the authors and should not be interpreted as representing the official views or policies of the Department of Defense or the U.S. Government. W. W. H. is supported in part by the Stanford Institute of Theoretical Physics. Numerical simulations were performed on Stanford Research Computing Center's Sherlock cluster. This project originated from discussions at the KITP programs *"Energy and Information Transport in Non-Equilibrium Quantum Systems"* and *"Non-Equilibrium Universality: From Classical to Quantum and Back"*; KITP is supported by the National Science Foundation under Grant No. NSF PHY-1748958.

Appendix A: Monotonicity of distances and design times

In this Appendix we show that the distances to the uniform ensemble $\Delta_\alpha^{(k)}$, Eq. (12), obey monotonicity: $\Delta_\alpha^{(k+1)} \geq \Delta_\alpha^{(k)}$, for indices $\alpha = 1$ (trace norm), $\alpha = 2$ (Frobenius norm), and $\alpha = \infty$ (operator norm). Understanding for which other values of α this property holds is an interesting direction for future work.

A consequence of the monotonicity of the distances $\{\Delta_\alpha^{(k)}\}$ is that the design times $\{t_{k,\alpha}\}$ as defined in Eq. (16) also obey monotonicity, i.e., they are non-decreasing in k for such indices. This is a desirable property that allows the interpretation of the design times as a sequence of time scales describing progressively "deeper" levels of thermalization.

1. $\alpha = 1$ (trace norm)

This choice, recently used in Refs. [4, 5], corresponds to (twice) the trace distance $D(\rho,\sigma) \equiv \frac{1}{2}\|\rho-\sigma\|_1$. Using the fact that $\rho^{(k)} = \Phi[\rho^{(k+1)}]$, where Φ is the quantum channel representing erasure (i.e. partial trace) of a replica, and the data-processing inequality for the trace distance, we have

$$\begin{aligned}\Delta_1^{(k+1)} &= 2D(\rho^{(k+1)}, \rho_H^{(k+1)}) \\ &\geq 2D(\Phi[\rho^{(k+1)}], \Phi[\rho_H^{(k+1)}]) = 2D(\rho^{(k)}, \rho_H^{(k)}) \\ &= \Delta_1^{(k)} \ . \end{aligned} \tag{A1}$$

2. $\alpha = 2$ (Frobenius norm)

This is the choice we use in this work. We use the data-processing inequality for the *"sandwiched Renyi entropy"* [84]

$$D_\alpha(\rho\|\sigma) = \frac{1}{\alpha-1}\ln \mathrm{Tr}\Big[(\sigma^{\frac{1-\alpha}{2\alpha}}\rho\sigma^{\frac{1-\alpha}{2\alpha}})^\alpha\Big] \tag{A2}$$

with $\rho = \rho^{(k)}$ and $\sigma = \rho_H^{(k)}$ (note the support of ρ is included in the support of σ, i.e. the symmetric sector of the k-fold replicated Hilbert space). We have

$$D_2(\rho^{(k)}\|\rho_H^{(k)}) = \ln \frac{\mathrm{Tr}\big[(\rho^{(k)})^2\big]}{F_H^{(k)}} = \ln \frac{F^{(k)}}{F_H^{(k)}}. \tag{A3}$$

Thus the data-processing inequality $D_2(\Phi[\rho]\|\Phi[\sigma]) \leq D_2(\rho\|\sigma)$ for the erasure of a replica yields

$$\frac{F^{(k+1)}}{F_H^{(k+1)}} \geq \frac{F^{(k)}}{F_H^{(k)}}. \tag{A4}$$

and finally $\Delta_2^{(k+1)} \geq \Delta_2^{(k)}$.

3. $\alpha = \infty$ (operator norm)

This choice, employed e.g. in Refs. [7, 31], corresponds to the operator norm $\|\rho\|_\infty = \max\{|\lambda|\}$, where $\{\lambda\}$ is the spectrum of ρ. Using the fact that $\rho_H^{(k)} = F_H^{(k)}\Pi_{\mathrm{symm}}$, and that $\rho^{(k)}$ is supported inside Π_{symm} (projector on the symmetric sector of the replicated Hilbert space), the condition $\Delta_\infty^{(k)} < \epsilon$ can be rewritten as

$$\|\rho^{(k)}/F_H^{(k)} - \Pi_{\mathrm{symm}}\|_\infty < \epsilon \tag{A5}$$

i.e. $\lambda \in [F_H^{(k)}(1-\epsilon), F_H^{(k)}(1+\epsilon)]$ for all eigenvalues λ of $\rho^{(k)}$ (except the zero eigenvalues in the orthogonal complement of Π_{symm}). In turn, this condition can be rewritten as

$$(1-\epsilon)\rho_H^{(k)} \leq \rho^{(k)} \leq (1+\epsilon)\rho_H^{(k)} \tag{A6}$$

(the form used in Ref. [7]). Thus by tracing out a replica one sees that an ϵ-approximate $(k+1)$-design is also an ϵ-approximate k-design.

Appendix B: Existence of a limit state

In this Appendix we prove some results that are used towards showing the existence of a limit state $\rho_\infty^{(k)}$ in Sec. III.

We begin by remarking on the structure of channels $\mathcal{D}'_r$ from Eq. (21). First of all, these channels are unitarily equivalent to $\mathcal{D}[\rho] = \frac{1}{4}\sum_\alpha K_\alpha \rho K_\alpha^\dagger$, with $K_\alpha = (\sigma_t^\alpha)^{\otimes k}$; we focus on the channel $\mathcal{D}$ in the following. We may decompose the state ρ into Pauli strings on the k-fold replicated spin chain, and note that the Kraus operators $K_\alpha = (\sigma_t^\alpha)^{\otimes k}$ (for $\alpha = x, y, z$) are three of these basis operators. Now, Pauli strings either commute or anticommute with each K_α. Let $OK_\alpha = (-1)^{s_\alpha}K_\alpha O$, $s_\alpha \in \mathbb{Z}_2$; by using the fact that $K_xK_yK_z \propto I^{\otimes k}$, we have $s_x \oplus s_y \oplus s_z = 0$ (sum is modulo 2). Thus we see immediately that the only possible scenarios are $\mathbf{s} = (0,0,0)$ or $\mathbf{s} = (1,1,0)$ and its permutations.

Thus the basis of Pauli strings can be partitioned into four sets: operators O_{all} that commute with *all* K_α's; operators $O_{0,\mathrm{x}}$ that commute with K_0 and K_x while anticommuting with K_y and K_z; and similarly-defined operators $O_{0,\mathrm{y}}$ and $O_{0,\mathrm{z}}$. A density matrix can be uniquely decomposed into

$$\rho = \rho_{\mathrm{all}} + \sum_{\alpha=x,y,z}\rho_{0,\alpha} \ . \tag{B1}$$

It is immediate to verify the following statements (recall $\|A\|_F = \sqrt{\mathrm{Tr}(A^\dagger A)}$ is the Frobenius norm):

$$\mathcal{D}[\rho] = \rho_{\mathrm{all}} \tag{B2}$$

$$\|\rho\|_F^2 = \|\rho_{\mathrm{all}}\|_F^2 + \sum_{\alpha=x,y,z}\|\rho_{0,\alpha}\|_F^2 \tag{B3}$$

From these it follows that

$$\|\rho\|_F^2 - \|\mathcal{D}[\rho]\|_F^2 = \|\rho - \mathcal{D}[\rho]\|_F^2 \ . \tag{B4}$$

Lemma. *Every circuit instance admits a limit state* $\rho_\infty^{(k)} = \lim_{N_B\to\infty}\rho^{(k)}$.

Proof. As $\mathcal{D}'_r$ are quantum channels, the sequence of 2-norms $\{n_r \equiv \|\rho_r^{(k)}\|_F : r \in \mathbb{N}\}$ is non-increasing. It is also bounded from below, thus it has a finite limit for $r \to \infty$ (its infimum). By using Eq. (B4), we have

$$n_r^2 - n_{r+1}^2 = \|\rho_r^{(k)} - \mathcal{D}'_r[\rho_r^{(k)}]\|_F^2 = \|\rho_r^{(k)} - \rho_{r+1}^{(k)}\|_F^2 \tag{B5}$$

Thus the states $\{\rho_r^{(k)}\}$ form a Cauchy sequence, which converges (since the space of states is metrically complete) to a limit state $\rho_\infty^{(k)}$. ■

Corollary. *In every circuit instance,* $\|[\rho_r^{(k)}, K_\alpha(r)]\|_F \to 0$ *as* $r \to \infty$.

Proof. It follows from Eq. (B5) that $\lim_{r\to\infty} \|(\rho_r^{(k)})_{0,\alpha}\|_F = 0$ for all $\alpha = x, y, z$. Since

$$\begin{aligned}[\rho_r^{(k)}, K_x(r)] &= \left(\rho_r^{(k)} - K_x(r)\rho_r^{(k)}K_x(r)\right) K_x(r) \\ &= \left[(\rho_r^{(k)})_{0,y} + (\rho_r^{(k)})_{0,z}\right] K_x(r) \end{aligned} \tag{B6}$$

(and similarly for the commutators with K_y and K_z), the conclusion follows. ■

Appendix C: Lemmas on universal gate sets

In this Appendix we prove some results used to prove the emergence of exact state designs in Sec. III, having to do with universality of the gate set G.

We begin by defining a slightly modified notion of universality for a gate set:

Definition. *A set* $G \subset U(4)$ *of two-qubit gates is* "brickwork-universal" *if the set of brickwork circuits on* N *qubits, with open boundary conditions, composed of gates in* G*, is dense in the unitary group* $U(2^N)$.

Note that this notion is more restrictive than conventional universality [10], as it imposes a restriction on the architecture of the circuit to be used to approximate arbitrary unitaries. Next, we show that open subsets $G \subset \mathfrak{DU}$ as considered in Sec. III fall within this definition:

Lemma. *Any open subset* $G \subset \mathfrak{DU}$ *is a brickwork-universal gate set.*

Proof. Let us take any gate $U \in G$ and build a brickwork layer $\mathbb{U} = (\mathbb{I} \otimes U^{\otimes N/2-1} \otimes \mathbb{I}) \cdot U^{\otimes N/2}$ (where $\mathbb{I}$ is the single-qubit identity and we take N to be even). This is a unitary matrix with eigenphases $\{\phi_n : \ n = 1, \dots 2^N\}$. The distance of the time evolution $\mathbb{U}^t$ from the identity is given by $2\sum_n[1 - \cos(\phi_n t)]$, a quasiperiodic (or possibly periodic) function. This distance can be made arbitrarily small by choosing a suitable $t = T \in \mathbb{N}$, according to the theory of Poincaré recurrence; thus $\mathbb{U}^T =_\epsilon \mathbb{I}^{\otimes N}$, where $=_\epsilon$ denotes equality up to error ϵ. By exploiting the fact that G is an open set, we can now make small changes to the parameters of the gate U at one of the bonds that are acted upon in the final time step[10], say $(i, i+1)$. We obtain a circuit $\mathbb{U}'\mathbb{U}^{T-1} =_\epsilon \mathbb{U}'\mathbb{U}^\dagger$ where $\mathbb{U}'$ is the modified final time step. Using the parametrization of dual-unitary gates $U = r_1 \otimes s_2 \cdot \mathsf{SWAP} \cdot e^{-iJZ_1Z_2} \cdot u_1 \otimes v_2$ $(r, s, u, v \in SU(2),\ J \in \mathbb{R})$, we see that we may weakly change r, s and J (while remaining in the open set G) to obtain

$$\begin{aligned}\mathbb{U}'\mathbb{U}^\dagger &= r'_i \otimes s'_{i+1} \cdot e^{-i(J'-J)Z_iZ_{i+1}} \cdot r_i^\dagger \otimes s_{i+1}^\dagger \\ &= (r'r^\dagger)_i \otimes (s's^\dagger)_{i+1} \cdot e^{-i(J'-J)(rZr^\dagger)_i(sZs^\dagger)_{i+1}}\,. \end{aligned} \tag{C1}$$

This shows that gates in G can generate arbitrary single-qubit rotations on any site[11], as well as entangling operations on half the bonds (recall that the parity of i here is fixed). The same reasoning with a small perturbation at the initial (rather than final) time yields entangling operations on the remaining bonds. Thus the gate set G is brickwork-universal. ■

Note that, as we did not vary the gates u and v, so the assumption that G be an open subset of $\mathfrak{DU}$ can be further tightened.

Circuits built out of brickwork-universal gate sets can approximate any unitary, by definition. In the following, we show that *random* circuits built out of such gates in fact approximate every element of the unitary group almost surely, as the circuit depth goes to infinity.

Lemma. *Let* B_ϵ *be an* ϵ*-ball in* $U(2^N)$*. Given a probability distribution* P *over a brickwork-universal gate set* G*, let* u *be a brickwork circuit on* N *qubits of infinite depth (i.e., semi-infinite in the time direction) generated by sampling the gates independently and identically from* P*. Let* $u(t)$ *be the truncation of* u *to depth* t*. Then, the sequence* $\{u(t) : t \in \mathbb{N}\}$ *visits* B_ϵ *almost surely.*

Proof. Let B_ϵ be centered around a unitary V. Since the gate set G is brickwork-universal, V can be decomposed, up to accuracy ϵ, into a brickwork circuit of gates in G with finite depth[12] t_c (this is the gate complexity of V relative to G). Thus the probability that $u(t_c) \in B_\epsilon$ is lower-bounded by the probability of randomly sampling the gate decomposition of V (exactly or within ϵ approximation, depending whether G is discrete or continuous). Let us call this probability $p(V) > 0$, and let us define $p_{\min} = \min_V p(V)$ (note $p_{\min} > 0$ as the unitary group is compact). This means that, if we take T as the maximum gate complexity of any element of $U(2^N)$, over a depth T there is a finite probability (bounded below by $p_{\min} > 0$) that the sequence $\{u(t) : t = nT + 1, \dots (n+1)T\}$ visits B_ϵ, $\forall n$. The probability that this doesn't happen over a time t is thus bounded above by $(1 - p_{\min})^{\lfloor t/T \rfloor} \sim e^{-(p_{\min}/T)t}$. Thus for $t \to \infty$ the ball B_ϵ is visited with probability 1. ■

[10] For this bond to be acted on at the final time, i must have a fixed parity.

[11] The gates $r'r^\dagger$, $s's^\dagger$ are small rotations, but by taking sufficiently high powers one can generate any single-qubit rotation.

[12] Note that this depth scales exponentially in the number of qubits N, but here we take N to be a finite constant.

Appendix D: Bounds on the purity of moments

Eq. (27) can be proven by using the convexity of $f(x) = x^k$ for all $k \geq 2$. Let the ensemble be $\mathcal{E} = \{p_i, |i\rangle\}$; then

$$\begin{aligned}\mathrm{Tr}\Big(\rho^{(k)^2}\Big) &= \sum_{i,j} p_i p_j \left|\langle i|j\rangle\right|^{2k} = \sum_{i,j} p_i p_j f(|\langle i|j\rangle|^2) \\ &\geq f\left(\sum_{i,j} p_i p_j \left|\langle i|j\rangle\right|^2\right) = \Big[\mathrm{Tr}\Big(\rho^{(1)^2}\Big)\Big]^k .\end{aligned} \tag{D1}$$

Eq. (28) can be derived by making use of Hölder's inequality: Let $a, b > 1$ such that $1/a + 1/b = 1$. Then we have

$$\sum_n |x_n y_n| \leq \left(\sum_n |x_n|^a\right)^{\frac{1}{a}} \left(\sum_n |y_n|^b\right)^{\frac{1}{b}}, \tag{D2}$$

for $x_n, y_n \in \mathbb{R}$ or $\mathbb{C}$. To use this, let $x_i = p(i)^{\frac{2}{k}} f(i)$ and $y_i = p(i)^{1-\frac{2}{k}}$. We choose $a = k$, so that $b = \frac{k}{k-1}$. Since all quantities are non-negative we can drop the absolute values and obtain

$$\sum_i p(i) f(i) \leq \left(\sum_i p(i)^2 f(i)^k\right)^{\frac{1}{k}} \left(\sum_i p(i)^{\frac{k-2}{k-1}}\right)^{\frac{k-1}{k}} . \tag{D3}$$

Now, by concavity of $g(x) = x^{\frac{1}{k-1}}$ $(k \geq 2)$ we have $\sum_i p(i)^{\frac{k-2}{k-1}} = \mathbb{E}_i[g(1/p(i))] \leq g[\mathbb{E}_i(1/p(i))] = M^{\frac{1}{k-1}}$. Thus,

$$\sum_i p(i) f(i) \leq \left(M \sum_i p(i)^2 f(i)^k\right)^{\frac{1}{k}} . \tag{D4}$$

Taking the k-th power of both sides yields Eq. (28). ■

[1] M. Srednicki, Chaos and quantum thermalization, Physical Review E **50**, 888 (1994).

[2] M. Rigol, V. Dunjko, and M. Olshanii, Thermalization and its mechanism for generic isolated quantum systems, Nature **452**, 854 (2008).

[3] L. D'Alessio, Y. Kafri, A. Polkovnikov, and M. Rigol, From quantum chaos and eigenstate thermalization to statistical mechanics and thermodynamics, Advances in Physics **65**, 239 (2016).

[4] J. Choi, A. L. Shaw, I. S. Madjarov, X. Xie, J. P. Covey, J. S. Cotler, D. K. Mark, H.-Y. Huang, A. Kale, H. Pichler, F. G. S. L. Brandão, S. Choi, and M. Endres, Emergent Randomness and Benchmarking from Many-Body Quantum Chaos, arXiv:2103.03535 [cond-mat, physics:physics, physics:quant-ph] (2021).

[5] J. S. Cotler, D. K. Mark, H.-Y. Huang, F. Hernandez, J. Choi, A. L. Shaw, M. Endres, and S. Choi, Emergent quantum state designs from individual many-body wavefunctions, arXiv:2103.03536 [cond-mat, physics:hep-th, physics:physics, physics:quant-ph] (2021).

[6] J. M. Renes, R. Blume-Kohout, A. J. Scott, and C. M. Caves, Symmetric informationally complete quantum measurements, Journal of Mathematical Physics **45**, 2171 (2004).

[7] A. Ambainis and J. Emerson, Quantum t-designs: t-wise Independence in the Quantum World, in *Twenty-Second Annual IEEE Conference on Computational Complexity (CCC'07)* (2007) pp. 129–140.

[8] W. W. Ho and S. Choi, Exact Emergent Quantum State Designs from Quantum Chaotic Dynamics, Physical Review Letters **128**, 060601 (2022).

[9] P. W. Claeys and A. Lamacraft, Emergent quantum state designs and biunitarity in dual-unitary circuit dynamics, arXiv:2202.12306 [cond-mat, physics:nlin, physics:quant-ph] (2022).

[10] A. Barenco, C. H. Bennett, R. Cleve, D. P. DiVincenzo, N. Margolus, P. Shor, T. Sleator, J. A. Smolin, and H. Weinfurter, Elementary gates for quantum computation, Physical Review A **52**, 3457 (1995).

[11] M. J. Gullans and D. A. Huse, Dynamical Purification Phase Transition Induced by Quantum Measurements, Physical Review X **10**, 041020 (2020).

[12] B. Skinner, J. Ruhman, and A. Nahum, Measurement-Induced Phase Transitions in the Dynamics of Entanglement, Physical Review X **9**, 031009 (2019).

[13] Y. Li, X. Chen, and M. P. A. Fisher, Quantum Zeno effect and the many-body entanglement transition, Physical Review B **98**, 205136 (2018).

[14] Y. Li, X. Chen, and M. P. A. Fisher, Measurement-driven entanglement transition in hybrid quantum circuits, Physical Review B **100**, 134306 (2019).

[15] A. Chan, R. M. Nandkishore, M. Pretko, and G. Smith, Unitary-projective entanglement dynamics, Phys. Rev. B **99**, 224307 (2019).

[16] P. Hayden and J. Preskill, Black holes as mirrors: quantum information in random subsystems, Journal of High Energy Physics **2007**, 120 (2007).

[17] P. Hosur, X.-L. Qi, D. A. Roberts, and B. Yoshida, Chaos in quantum channels, Journal of High Energy Physics **2016**, 4 (2016).

[18] D. A. Roberts and B. Yoshida, Chaos and complexity by design, Journal of High Energy Physics **2017**, 121 (2017).

[19] A. Nahum, S. Vijay, and J. Haah, Operator Spreading in Random Unitary Circuits, Physical Review X **8**, 021014 (2018).

[20] C. W. von Keyserlingk, T. Rakovszky, F. Pollmann, and

S. L. Sondhi, Operator Hydrodynamics, OTOCs, and Entanglement Growth in Systems without Conservation Laws, Physical Review X **8**, 021013 (2018).

[21] X. Mi, P. Roushan, C. Quintana, S. Mandrà, J. Marshall, C. Neill, F. Arute, K. Arya, J. Atalaya, R. Babbush, J. C. Bardin, R. Barends, J. Basso, A. Bengtsson, S. Boixo, A. Bourassa, M. Broughton, B. B. Buckley, D. A. Buell, B. Burkett, N. Bushnell, Z. Chen, B. Chiaro, R. Collins, W. Courtney, S. Demura, A. R. Derk, A. Dunsworth, D. Eppens, C. Erickson, E. Farhi, A. G. Fowler, B. Foxen, C. Gidney, M. Giustina, J. A. Gross, M. P. Harrigan, S. D. Harrington, J. Hilton, A. Ho, S. Hong, T. Huang, W. J. Huggins, L. B. Ioffe, S. V. Isakov, E. Jeffrey, Z. Jiang, C. Jones, D. Kafri, J. Kelly, S. Kim, A. Kitaev, P. V. Klimov, A. N. Korotkov, F. Kostritsa, D. Landhuis, P. Laptev, E. Lucero, O. Martin, J. R. McClean, T. McCourt, M. McEwen, A. Megrant, K. C. Miao, M. Mohseni, S. Montazeri, W. Mruczkiewicz, J. Mutus, O. Naaman, M. Neeley, M. Newman, M. Y. Niu, T. E. O'Brien, A. Opremcak, E. Ostby, B. Pato, A. Petukhov, N. Redd, N. C. Rubin, D. Sank, K. J. Satzinger, V. Shvarts, D. Strain, M. Szalay, M. D. Trevithick, B. Villalonga, T. White, Z. J. Yao, P. Yeh, A. Zalcman, H. Neven, I. Aleiner, K. Kechedzhi, V. Smelyanskiy, and Y. Chen, Information scrambling in quantum circuits, Science **374**, 1479 (2021).

[22] H. Kim and D. A. Huse, Ballistic Spreading of Entanglement in a Diffusive Nonintegrable System, Physical Review Letters **111**, 127205 (2013).

[23] A. Nahum, J. Ruhman, S. Vijay, and J. Haah, Quantum Entanglement Growth under Random Unitary Dynamics, Physical Review X **7**, 031016 (2017).

[24] S. H. Shenker and D. Stanford, Black holes and the butterfly effect, Journal of High Energy Physics **2014**, 67 (2014).

[25] H. Wilming and I. Roth, High-temperature thermalization implies the emergence of quantum state designs, arXiv:2202.01669 [cond-mat, physics:math-ph, physics:quant-ph] (2022).

[26] R. Nandkishore and D. A. Huse, Many-Body Localization and Thermalization in Quantum Statistical Mechanics, Annual Review of Condensed Matter Physics **6**, 15 (2015).

[27] D. A. Abanin, E. Altman, I. Bloch, and M. Serbyn, Colloquium: Many-body localization, thermalization, and entanglement, Reviews of Modern Physics **91**, 021001 (2019).

[28] E. Altman, K. R. Brown, G. Carleo, L. D. Carr, E. Demler, C. Chin, B. DeMarco, S. E. Economou, M. A. Eriksson, K.-M. C. Fu, M. Greiner, K. R. Hazzard, R. G. Hulet, A. J. Kollár, B. L. Lev, M. D. Lukin, R. Ma, X. Mi, S. Misra, C. Monroe, K. Murch, Z. Nazario, K.-K. Ni, A. C. Potter, P. Roushan, M. Saffman, M. Schleier-Smith, I. Siddiqi, R. Simmonds, M. Singh, I. Spielman, K. Temme, D. S. Weiss, J. Vučković, V. Vuletić, J. Ye, and M. Zwierlein, Quantum Simulators: Architectures and Opportunities, PRX Quantum **2**, 017003 (2021).

[29] S. Goldstein, J. L. Lebowitz, R. Tumulka, and N. Zanghì, On the Distribution of the Wave Function for Systems in Thermal Equilibrium, Journal of Statistical Physics **125**, 1193 (2006).

[30] S. Goldstein, J. L. Lebowitz, C. Mastrodonato, R. Tumulka, and N. Zanghì, Universal Probability Distribution for the Wave Function of a Quantum System Entangled with its Environment, Communications in Mathematical Physics **342**, 965 (2016).

[31] R. A. Low, Pseudo-randomness and learning in quantum computation, arXiv:1006.5227 [physics:quant-ph] (2010).

[32] M. C. Bañuls, M. B. Hastings, F. Verstraete, and J. I. Cirac, Matrix Product States for Dynamical Simulation of Infinite Chains, Phys. Rev. Lett. **102**, 240603 (2009).

[33] M. B. Hastings and R. Mahajan, Connecting entanglement in time and space: Improving the folding algorithm, Phys. Rev. A **91**, 032306 (2015).

[34] A. Lerose, M. Sonner, and D. A. Abanin, Influence Matrix Approach to Many-Body Floquet Dynamics, Physical Review X **11**, 021040 (2021).

[35] S. J. Garratt and J. T. Chalker, Local Pairing of Feynman Histories in Many-Body Floquet Models, Physical Review X **11**, 021051 (2021).

[36] M. Ippoliti and V. Khemani, Postselection-Free Entanglement Dynamics via Spacetime Duality, Physical Review Letters **126**, 060501 (2021).

[37] M. Ippoliti, T. Rakovszky, and V. Khemani, Fractal, Logarithmic, and Volume-Law Entangled Nonthermal Steady States via Spacetime Duality, Physical Review X **12**, 011045 (2022).

[38] T.-C. Lu and T. Grover, Spacetime duality between localization transitions and measurement-induced transitions, PRX Quantum **2**, 040319 (2021).

[39] S. J. Garratt and J. T. Chalker, Many-Body Delocalization as Symmetry Breaking, Physical Review Letters **127**, 026802 (2021).

[40] C. Jonay, V. Khemani, and M. Ippoliti, Triunitary quantum circuits, Physical Review Research **3**, 043046 (2021).

[41] B. Bertini, K. Klobas, V. Alba, G. Lagnese, and P. Calabrese, Growth of R\'enyi Entropies in Interacting Integrable Models and the Breakdown of the Quasiparticle Picture, arXiv:2203.17264 [cond-mat, physics:hep-th, physics:quant-ph] (2022).

[42] M. Akila, D. Waltner, B. Gutkin, and T. Guhr, Particle-time duality in the kicked Ising spin chain, Journal of Physics A: Mathematical and Theoretical **49**, 375101 (2016).

[43] B. Bertini, P. Kos, and T. Prosen, Exact Spectral Form Factor in a Minimal Model of Many-Body Quantum Chaos, Physical Review Letters **121**, 264101 (2018).

[44] S. Gopalakrishnan and A. Lamacraft, Unitary circuits of finite depth and infinite width from quantum channels, Physical Review B **100**, 064309 (2019).

[45] P. W. Claeys and A. Lamacraft, Maximum velocity quantum circuits, Physical Review Research **2**, 033032 (2020).

[46] B. Bertini, P. Kos, and T. Prosen, Entanglement Spreading in a Minimal Model of Maximal Many-Body Quantum Chaos, Physical Review X **9**, 021033 (2019).

[47] B. Bertini, P. Kos, and T. Prosen, Exact Correlation Functions for Dual-Unitary Lattice Models in 1+1 Dimensions, Physical Review Letters **123**, 210601 (2019).

[48] B. Bertini and L. Piroli, Scrambling in random unitary circuits: Exact results, Physical Review B **102**, 064305 (2020).

[49] P. Kos, B. Bertini, and T. Prosen, Correlations in Perturbed Dual-Unitary Circuits: Efficient Path-Integral Formula, Physical Review X **11**, 011022 (2021).

[50] L. Piroli, B. Bertini, J. I. Cirac, and T. Prosen, Exact dynamics in dual-unitary quantum circuits, Physical Review B **101**, 094304 (2020).

[51] P. W. Claeys and A. Lamacraft, Ergodic and Nonergodic Dual-Unitary Quantum Circuits with Arbitrary Local Hilbert Space Dimension, Physical Review Letters **126**, 100603 (2021).

[52] B. Bertini, P. Kos, and T. Prosen, Random Matrix Spectral Form Factor of Dual-Unitary Quantum Circuits, Communications in Mathematical Physics **387**, 597 (2021).

[53] S. A. Rather, S. Aravinda, and A. Lakshminarayan, Creating Ensembles of Dual Unitary and Maximally Entangling Quantum Evolutions, Physical Review Letters **125**, 070501 (2020).

[54] B. Gutkin, P. Braun, M. Akila, D. Waltner, and T. Guhr, Local correlations in dual-unitary kicked chains, arXiv:2001.01298 [cond-mat, physics:math-ph, physics:nlin] (2020).

[55] M. J. Gullans and D. A. Huse, Scalable Probes of Measurement-Induced Criticality, Physical Review Letters **125**, 070606 (2020).

[56] Y. Bao, S. Choi, and E. Altman, Theory of the phase transition in random unitary circuits with measurements, Physical Review B **101**, 104301 (2020).

[57] S. Choi, Y. Bao, X.-L. Qi, and E. Altman, Quantum Error Correction in Scrambling Dynamics and Measurement-Induced Phase Transition, Physical Review Letters **125**, 030505 (2020).

[58] C.-M. Jian, Y.-Z. You, R. Vasseur, and A. W. W. Ludwig, Measurement-induced criticality in random quantum circuits, Physical Review B **101**, 104302 (2020).

[59] M. Ippoliti, M. J. Gullans, S. Gopalakrishnan, D. A. Huse, and V. Khemani, Entanglement Phase Transitions in Measurement-Only Dynamics, Physical Review X **11**, 011030 (2021).

[60] A. Lavasani, Y. Alavirad, and M. Barkeshli, Measurement-induced topological entanglement transitions in symmetric random quantum circuits, Nature Physics **17**, 342 (2021).

[61] L. Fidkowski, J. Haah, and M. B. Hastings, How Dynamical Quantum Memories Forget, Quantum **5**, 382 (2021).

[62] R. Fan, S. Vijay, A. Vishwanath, and Y.-Z. You, Self-organized error correction in random unitary circuits with measurement, Phys. Rev. B **103**, 174309 (2021).

[63] A. Lavasani, Y. Alavirad, and M. Barkeshli, Topological Order and Criticality in $(2+1)\mathrm{D}$ Monitored Random Quantum Circuits, Physical Review Letters **127**, 235701 (2021), publisher: American Physical Society.

[64] M. Szyniszewski, A. Romito, and H. Schomerus, Universality of Entanglement Transitions from Stroboscopic to Continuous Measurements, Phys. Rev. Lett. **125**, 210602 (2020).

[65] A. Nahum and B. Skinner, Entanglement and dynamics of diffusion-annihilation processes with Majorana defects, Physical Review Research **2**, 023288 (2020).

[66] A. Nahum, S. Roy, B. Skinner, and J. Ruhman, Measurement and Entanglement Phase Transitions in All-To-All Quantum Circuits, on Quantum Trees, and in Landau-Ginsburg Theory, PRX Quantum **2**, 010352 (2021).

[67] Y. Li and M. P. A. Fisher, Statistical mechanics of quantum error correcting codes, Physical Review B **103**, 104306 (2021).

[68] Y. Li, S. Vijay, and M. P. A. Fisher, Entanglement Domain Walls in Monitored Quantum Circuits and the Directed Polymer in a Random Environment, arXiv:2105.13352 [cond-mat, physics:quant-ph] (2021).

[69] U. Agrawal, A. Zabalo, K. Chen, J. H. Wilson, A. C. Potter, J. H. Pixley, S. Gopalakrishnan, and R. Vasseur, Entanglement and charge-sharpening transitions in U(1) symmetric monitored quantum circuits, arXiv:2107.10279 [cond-mat, physics:quant-ph] (2021).

[70] A. C. Potter and R. Vasseur, Entanglement dynamics in hybrid quantum circuits, arXiv:2111.08018 [cond-mat, physics:quant-ph] (2021).

[71] T. Zhou and A. Nahum, Emergent statistical mechanics of entanglement in random unitary circuits, Phys. Rev. B **99**, 174205 (2019).

[72] T. Zhou and A. Nahum, Entanglement Membrane in Chaotic Many-Body Systems, Phys. Rev. X **10**, 031066 (2020).

[73] I. Marvian and R. W. Spekkens, A Generalization of Schur–Weyl Duality with Applications in Quantum Estimation, Communications in Mathematical Physics **331**, 431 (2014).

[74] B. Swingle, G. Bentsen, M. Schleier-Smith, and P. Hayden, Measuring the scrambling of quantum information, Phys. Rev. A **94**, 040302 (2016).

[75] C. Sünderhauf, L. Piroli, X.-L. Qi, N. Schuch, and J. I. Cirac, Quantum chaos in the Brownian SYK model with large finite N : OTOCs and tripartite information, Journal of High Energy Physics **2019**, 38 (2019).

[76] H. Gharibyan, M. Hanada, S. H. Shenker, and M. Tezuka, Onset of random matrix behavior in scrambling systems, Journal of High Energy Physics **2018**, 124 (2018).

[77] V. Alba and P. Calabrese, Entanglement and thermodynamics after a quantum quench in integrable systems, Proceedings of the National Academy of Sciences **114**, 7947 (2017).

[78] P. Calabrese, Entanglement spreading in non-equilibrium integrable systems, SciPost Physics Lecture Notes , 20 (2020).

[79] S. Gopalakrishnan, Operator growth and eigenstate entanglement in an interacting integrable Floquet system, Physical Review B **98**, 060302 (2018).

[80] K. Klobas, B. Bertini, and L. Piroli, Exact Thermalization Dynamics in the "Rule 54" Quantum Cellular Automaton, Physical Review Letters **126**, 160602 (2021).

[81] B. Buča, K. Klobas, and T. Prosen, Rule 54: exactly solvable model of nonequilibrium statistical mechanics, Journal of Statistical Mechanics: Theory and Experiment **2021**, 074001 (2021).

[82] Y. Bao, M. Block, and E. Altman, Finite time teleportation phase transition in random quantum circuits, arXiv:2110.06963 [cond-mat, physics:quant-ph] (2022).

[83] J. Napp, R. L. La Placa, A. M. Dalzell, F. G. S. L. Brandao, and A. W. Harrow, Efficient classical simulation of random shallow 2D quantum circuits, arXiv:2001.00021 [cond-mat, physics:quant-ph] (2020).

[84] R. L. Frank and E. H. Lieb, Monotonicity of a relative Rényi entropy, Journal of Mathematical Physics **54**, 122201 (2013).